GEOPHYSICAL CHARACTERIZATION OF FAULTS OF THE OKAVANGO RIFT ZONE, NORTHWEST BOTSWANA, AFRICA

By

KELSEY S. MOSLEY

Bachelor of Science in Geology

Oklahoma State University

Stillwater, Oklahoma

2010

Submitted to the Faculty of the
Graduate College of the
Oklahoma State University
in partial fulfillment of
the requirements for
the Degree of
MASTER OF SCIENCE
May, 2010

GEOPHYSICAL CHARACTERIZATION OF FAULTS

OF THE OKAVANGO RIFT ZONE, NORTHWEST

BOTSWANA, AFRICA

Thesis Approved:

Dr. Estella Atekwana

Thesis Adviser

Dr. Eliot Atekwana

Dr. Anna Cruse

Dr. A. Gordon Emslie

Dean of the Graduate College

ACKNOWLEDGMENTS

This research opportunity would not have been possible without my professor, mentor, and committee chair, Dr. Estella Atekwana of Oklahoma State University (OSU). Thank you for countless hours of instruction and guidance in helping me to become a better geoscientist. I am also grateful for my other committee members, Dr. Eliot Atekwana and Dr. Anna Cruse for your suggestions and advice in improving my thesis. I would like to extend a very special thank you to Dr. Kevin Mickus of Missouri State University (MSU) for assisting me with the geophysical components of my thesis. I also acknowledge Kristi Teter and Andrew Foreman for being excellent field partners while in Botswana.

This thesis was conducted as part of a National Science Foundation international research for students program (NSF-OISE-0644836). Special thanks to the Geological Survey of Botswana for providing the aeromagnetic data and gravity data for our study. I would like to extend my sincerest gratitude to the University of Botswana for providing our research team with logistical support while conducting field work in Botswana. I greatly appreciate our Botswana research partners: Dr. Motsoptse Modisi, Dr. Elisha Shemang, Dr. Loago Molwalefhe, and Dr. Moidaki Moikwathai (Dax) of the University of Botswana and their students: Banabotlhe Dikgang, Chicco Dance, and Elvis Mosweue for their time spent in the field collecting data and assisting me with the processing. I would also like to acknowledge Dr. Baraka Kinabo of the University of

Missouri-Rolla (UMR) (now at Chevron-Texaco) for his guidance in helping me continue his previous research.

I would like to thank Oklahoma State University and the Boone Pickens's School of Geology for providing me with an education that has prepared me for my future. I am grateful for all of the scholarships I have been blessed to earn, especially the John and Mildred Naff President's Distinguished Scholarship and the Devon Energy Fellowship, that assisted me in perusing my education. Special thanks to Dr. Todd Halihan for allowing me to use his software and geophysical equipment. Thank you to all of the professors who have impacted my life in a positive way and have helped me succeed as an undergraduate and graduate student. I appreciate all of my friends and geology family that continued to encourage me and bring joy to my life while attending OSU.

I am indebted to my mother and father for ALWAYS being a consistent source of encouragement and support. You all have instilled in me the qualities and characteristics I needed to excel in life. Thank you for your love, compassion, guidance, wisdom, and for implanting in me the belief that through Jesus Christ, all things are possible.

TABLE OF CONTENTS

Chapter Page

LIST OF FIGURES

Figure Page

Figure Page

CHAPTER I

INTRODUCTION

The Okavango Rift Zone (ORZ) has been suggested to be a zone of incipient continental rifting found at the terminal end of the Southwestern branch of the East African Rift System (EARS), therefore providing a unique opportunity to investigate fault characteristics related to early rifting processes. As such, the ORZ has been the focus of several shallow subsurface geologic (e.g., Modisi, 2000) and geophysical investigations (Modisi et al., 2000; Kinabo et al., 2007; Laletsang et al., 2007; Kinabo et al., 2008; Shemang and Molwalefhe, 2009). More recent studies have focused on understanding the interplay between neotectonics and surficial processes (e.g., Gamrod, 2009; Teeter, 2009) during the beginning stages of continental rifting to determine how environmental changes relate to climate and tectonics recorded in lake sediments associated with the rift.

Previous geoelectrical studies (e.g., Laletsang et al., 2007 and Shemang and Molwalefhe, 2009) have shown that some of the fault zones that comprise the ORZ consist of a number of synthetic and antithetic faults; however, penetration depths only reached between 80 m and 100 m below the surface. Hence information on the structure of the basin and subsurface character of the faults characterizing the rift is limited.

More recently, investigations by Kinabo et al. (2007;2008) have provided some

important insights into the growth and propagation of faults during the initial stage of rift formation. Using Shuttle Radar Tomography Mission, Digital Elevation Model (SRTM–DEM) and aeromagnetic data, Kinabo et al. (2008) compared the throw on individual faults as measured by the height of the fault scarps on the DEM images and the difference in depth to the tops of magnetic sources (basement) on the aeromagnetic maps and classified the faults in the ORZ into (a) old and active faults, (b) young and active faults, (c) faults with no recent activity, and (d) faults with waning activity. In particular, some faults showed considerable fault throws but lacked topographic scarps. Kinabo et al. (2008) suggested that the lack of surface expression for these basement faults may suggest the following: 1) lack of recent activity along these faults, 2) that these basement faults were reactivated, but are now concealed by rapid sedimentation associated with Okavango alluvial fan deposits, and 3) they were reactivated but lacked sufficient energy to rupture the surface (i.e., blind normal faults). The authors suggested that further geophysical studies were required in order to confirm the lack of activity along these faults. The study by Kinabo et al. (2008) also indicated that under lapping to overlapping segments observed on the surface along some faults may be connected twists in the basement. Hence, more work is required to provide data that can bridge the gap between the surface expression of these faults and their basement expression (i.e., how these faults link at depth).

These previous investigations provide important information on how faults grow and propagate through accommodating strain by linkage between individual fault segments in the basement and at the surface; however, some unanswered questions remain including: 1) as strain is transferred from older, less active faults in the interior of the rift to

younger, more active faults on the exterior of the rift (e.g., Kinabo et al., 2008) which faults are still actively participating in lengthening and widening of the rift, 2.) what is the reason for the differences in magnetic character of the faults in the basement (i.e., some of the faults within the ORZ are depicted as magnetic highs on aeromagnetic maps while others are depicted as magnetic lows), and 3.) is there a relationship between fluid flow from the Okavango Delta and fault development within the ORZ?

In this study, we extend the work of Kinabo et al. (2008) by examining the geophysical characteristics of the faults associated with the ORZ. Our specific objectives included: 1.) determining the subsurface fault geometry, 2.) depth extent of the faults, and 3.) elucidate the tectonic activity of the faults and the behavior the faults within the basement. By understanding these properties, possible implications on how fluid flow may influence the magnetic properties of the faults and if fluid flow is directly related to seismic activity from rift development can be derived. We investigated these properties using electrical resistivity tomography (ERT), magnetotellurics (MT), total field magnetic, and gravity surveys along selected faults characterizing the rift. Our results suggest that despite partial burial of some of the faults, majority of the faults associated with the ORZ have propagated through the sedimentary cover and are interpreted to be conducting fluids which suggests recent tectonic activity. Faults that are not conducting fluids may be experiencing cementation from past fluid flow and closure due to inactivity. These results suggest that the fault zones are acting as both conduits and barriers to fluid flow from the Okavango Delta. The differences in the magnetic character of the faults may be directly related to the occurrence of geochemical redox reactions between fluids being conducted along the faults and basement rocks. A second

cause may be that the faults juxtapose rocks of varying magnetic susceptibilities. Seismicity within the ORZ may be influenced by fluid flow within the fault zones. The ORZ lacks strong earthquakes. The lack of violent earthquakes may be due to fluid-filled pore space within the fault zones which increases pore pressure thus reducing the shear stress required for rupture, possibly allowing the rift to lengthen and widen more rapidly over time.

The findings of this study will add to the importance of understanding the interplay between fluid migration along fault planes and its influence on fault movement, magnetic characterization, and seismic activity.

CHAPTER II

GEOLOGIC SETTING

2.1 The East African Rift System

The East African Rift System (EARS) is an example of a classic continental rift zone. The rift system is traditionally divided into two branches, the older more evolved (>15 Ma) Eastern branch and the younger less evolved (<15 Ma) Western branch (Figure 1A). The Eastern rift extends from the Afar depression in Ethiopia in the north through the Kenya (Gregory) and Turkana rifts in Kenya to central Tanzania in the south (Chorowicz, 2005) where the rift terminates in a diffuse zone of extension within the Tanzanian craton. The Western rift extends from Lake Alberta in Uganda through western Tanzania where it forms basins including Lake Tanganyika, Lake Rukwa, and Lake Nyanza (Malawi) and continues towards the south of Dombe in Mozambique (Kampunzu et al., 1998).

The EARS occurs along a divergent plate boundary between the Nubian plate and the Somalian plate. Recent present day kinematic studies of the EARS (e.g., Stamps et al., 2008) suggest three subplates (Victoria, Rovuma, and Lwandle) and possibly a fourth plate (Transgariep) between the Nubian and Somalian plates (Figure 1C). Through the use of GPS solutions, the study concluded that plate angular velocities range from 1 to 6 mm/yr across the Western and Eastern rifts. Plate velocities increase from north to south

along the Western branch and from south to north for the Eastern branch. According to Stamps et al. (2008), the southward decrease of the extension rate along the Eastern branch is consistent with progressive disappearance of prominent active faults, as the Eastern branch propagates into cold cratonic domain.

The rift traverses two areas of continental uplift, the Ethiopian and Kenya domes, separated by the low-lying Turkana depression in northern Kenya. Throughout Ethiopia, the Eastern branch of the rift defines a single zone of extension and volcanic activity. The Western branch is separated into two branches that encircle the mechanically robust Tanzania craton (Furman, 2007). The earliest recorded volcanic activity in the EARS took place ~40 – 45 Ma in the northern Turkana depression (e.g., southernmost Ethiopia; Ochieng, 1988; Ebinger et al., 1993; George et al., 1998; Knight et al., 2003). However, the modern EARS magmatic province is generally described with respect to the onset of flood basalt activity in modern Ethiopia, Eritrea, and Yemen that occurred in the late Oligocene and is attributed to impact of a mantle plume head at the base of the lithosphere (Chorowicz, 2005; Furman, 2007). In both the Eastern and Western branches, volcanic provinces are older in the north than the south, with volcanic activity within the Eastern branch preceding those within the Western branch by ~11 Ma (Ebinger, 1989; Kampunzu et al., 1998). The mafic lavas erupted along the EARS display a wide range of geochemical and isotopic compositions that reflect heterogeneity in both source and process. The types of volcanism range from silica-undersaturated mafic lavas in the Western branch, where crustal extension is low, to transitional-tholeiitic basalts in the Eastern branch, where prolonged and intermediate degrees of extension are taking place (Furman, 2007). In contrast to the widespread volcanism

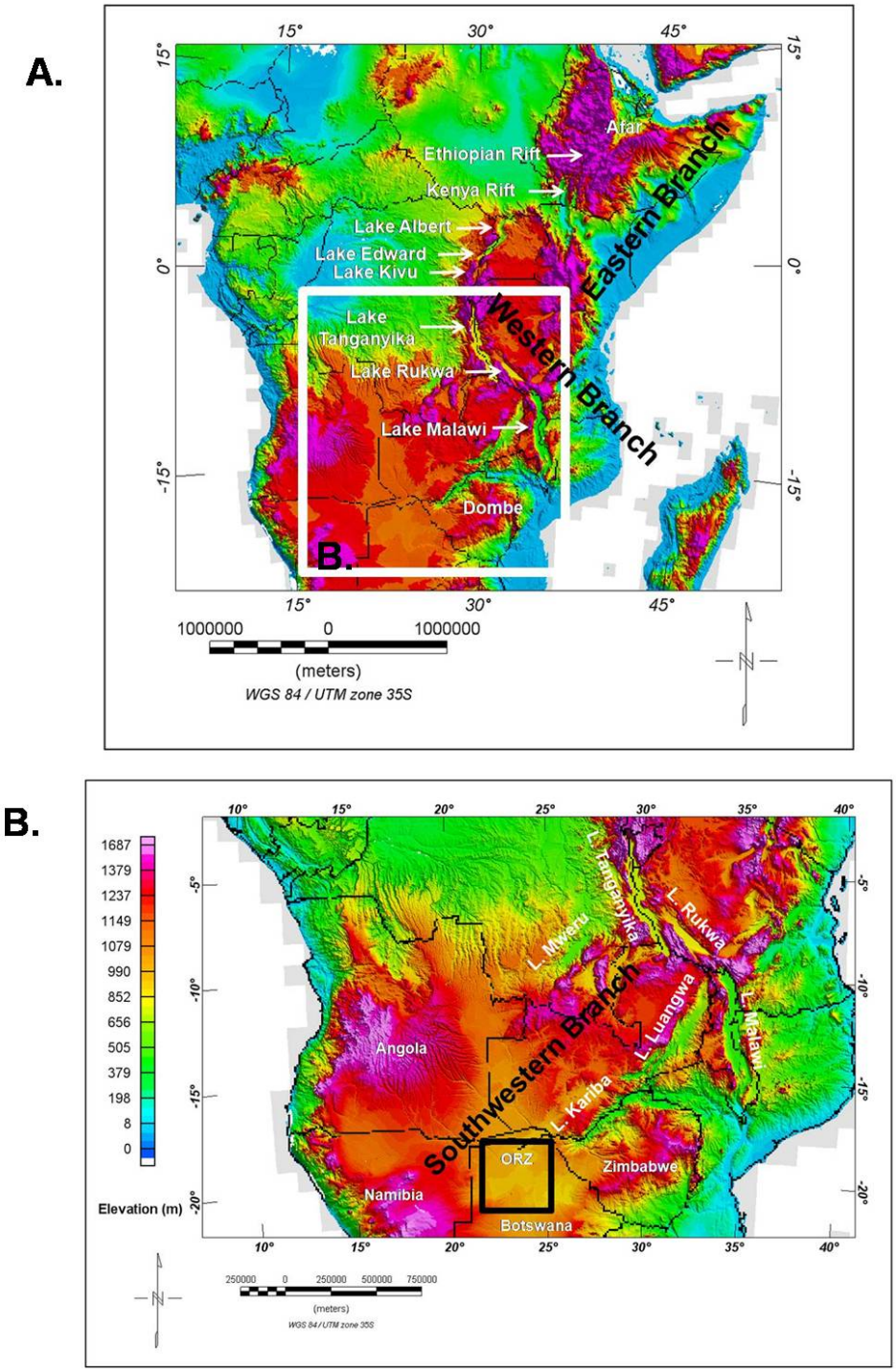

Figure 1. Maps displaying the location of the study area. A.) Shuttle Radar Tomography Mission, Digital Elevation Model (SRTM – DEM) of the East African Rift System (EARS). B.) SRTM-DEM map of the Southwestern Branch of the EARS. The black box shows the location of our study area.

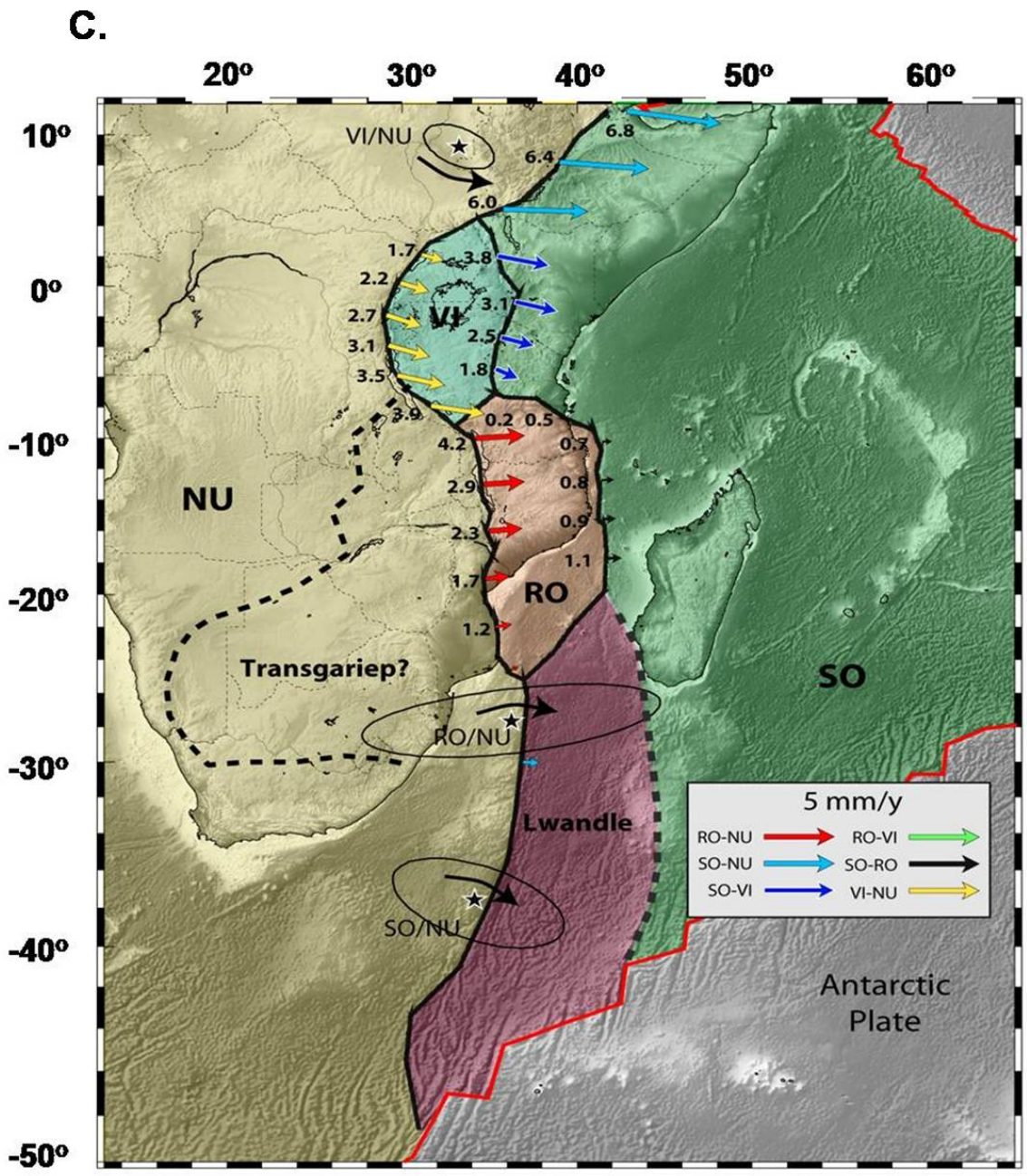

Figure 1 (cont). C.) Model showing the relative motion along plate or block boundaries within the EARS (courtesy of Dr. E. Calais, 2009).

observed in the Eastern rifts, the Western rifts are considered dry, as volcanic centers are aerially and volumetrically smaller (Ebinger, 2005).

The earliest extension documented in the EARS occurred in the Turkana area ~25 Ma (Morley et al., 1992; Hendrie et al., 1994). Volcanism and faulting propagated from this region to both the north and south, forming the familiar structures and rift basins of the modern rift branches (Furman, 2007). Structurally, the rifts are segmented along their lengths into a series of asymmetric half-grabens bounded by en-echelon curvilinear border faults. The individual rift basins (50 – 100 km long and 40 – 100 km wide) are linked by transfer faults/accommodation zones (Rosendahl, 1987; Ebinger, 1989; Chorowicz, 2005) and filled with fluvio-deltaic and lacustrine sediments and/or volcanics and volcaniclastics. The succession of graben basins are generally bordered on the two sides by high relief (100s of meters), comprising of almost continuous parallel mountain lines and plateaus, and sometimes volcanic massifs. Sediment fill and volcanic layers in the grabens range from < 1200 m to up to > 3 km (Chorowicz, 2005).

A third Southwestern branch (Figure 1B) (e.g., Fairhead and Girdler, 1969; Reeves, 1972; Girdler, 1975; Chapman and Pollack, 1977; Ballard et al., 1987; Sebaganzi et al., 1993; Modisi et al., 2000; Sebagenzi and Kaputo, 2002) consists of a network of separate Quaternary rift basins 100 km long and 40 – 80 km wide (Modisi et al., 2000) distributed along an approximately 250 km wide corridor extending for about 1700 km west of Lake Tanganyika and Lake Malawi with the Okavango Rift Zone (ORZ) at its southern-most extent in northwest Botswana (Kinabo et al., 2007). Very little is known about the structural and tectonic development of the Southwestern branch of the EARS.

The rate of extension is not known and the lack of surface magmatism prevents insights into possible lithospheric/asthenospheric processes occurring below the rift.

2.2. The Okavango Rift Zone

The Okavango Rift Zone (ORZ) (e.g., Kinabo et al., 2007; 2008) occurs in an intercratonic zone between the Congo craton to the northwest and the Zimbabwe and Kaapvaal cratons to the east-southeast. The rift is superimposed on the Ghanzi-Chobe belt, a Proterozoic orogenic province. Development of the ORZ is taking place within a large structural depression known as the Makgadikgadi-Okavango-Zambezi basin (MOZ) and is characterized by northeasterly trending folds and faults of the Ghanzi-Chobe belt (Cooke, 1984). A west-northwest trending dike swarm (the 179 Ma Karoo dike swarm) is superimposed on the faults of the Ghanzi-Chobe belt and is cut by younger normal faults associated with current rifting processes (Modisi et al., 2000). The ORZ consists of three grabens, paleo-Lake Ngami in the southwest and Mababe and Linyanti-Chobe in the northeast (Figure 2A). In the Lake Ngami graben, the northeast trending Tsau and Kunyere faults bound the graben to the northwest and southeast respectively. The Mababe basin is bounded by the Mababe Fault to the east while the Linyanti-Chobe graben is bounded by the Chobe Fault in the east and possibly an extension of the Gumare Fault in the west. The dips of the Gumare, Tsau, and Lecha faults are towards the southeast while the Kunyere, Thamalakane, Mababe, and Chobe faults are northwest dipping faults (Modisi et al., 2000; Kinabo et al., 2007). Sediment fill for both the Ngami and Mababe depressions may reach as deep as 700 m (Kinabo et al., 2007). Compared to the well developed grabens of the Eastern and Western branches of the EARS with fault

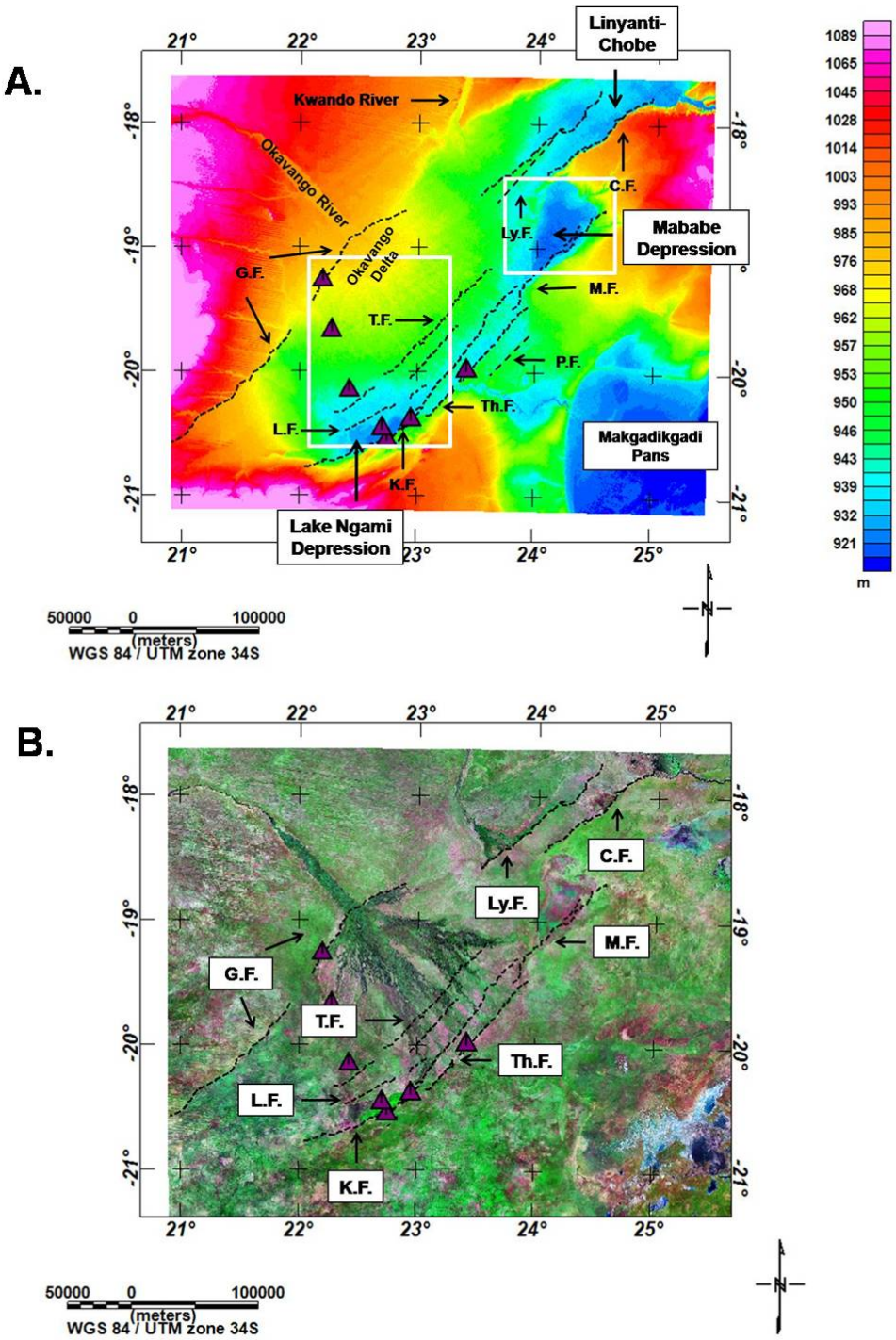

Figure 2. Maps of the Okavango Rift Zone (ORZ). A.) SRTM-DEM map of the ORZ. Dashed lines indicate the location of the faults. Triangles represent the location of towns and villages. White boxes delineate our study areas. The Tsau Fault (T.F.) and the Lecha Fault (L.F.) are not visible on the surface. Their locations were determined by magnetic data. B.) Terrain map of the ORZ showing the extent of the Okavango Delta. G.F. = Gumare Fault, Ly.F. = Linyanti Fault, C.F. = Chobe Fault, M.F. = Mababe Fault, T.F. = Tsau Fault, L.F. = Lecha Fault, K.F. = Kunyere Fault, Th.F. = Thamalakane Fault, and P.F. = Phuti Fault.

scarps reaching 100s of meters, fault scarp heights in the ORZ range from 6 m along Lake Ngami to 12 – 18 m in Mababe. Farther north, scarp heights increase to as much as 44 m in Linyanti-Chobe (Kinabo et al., 2008).

The strike of the main bounding rift-related faults is 030 – 050^{o} in the north and 060 – 070^{o} in the south (Kinabo et al., 2007;2008). The orientation of the faults on the surface is influenced by pre-existing faults and folds of the basement rocks (Modisi et al., 2000; Kinabo et al., 2007;2008). Fault growth and propagation is through strain accommodation from older, less active faults in the interior of the rift to younger, more active faults on the exterior of the rift and by hard-linkage (hooking, fused segments) and soft-linkage (under lapping to overlapping) of individual faults to establish a master border fault (Kinabo et al., 2008). As a result, strain accommodation along the major rift-related northeasterly-trending faults has caused subsidiary north-northwest-south-southeast trending faults and fractures to form. The spatial distribution of the main bounding rift-related faults and the subsidiary faults and fractures suggest a right-lateral strike-slip component in addition to the predominant dip-slip component associated with rift formation. The different sets of movement along the faults and fractures accommodate the regional east-west extension of the EARS (Modisi et al., 2000; Kinabo et al., 2008).

The ORZ hosts the largest inland alluvial fan on Earth, the Okavango Delta (Figure 2B), supporting the largest (~18,000 km^{2}) wetland in southern Africa (McCarthy et al., 1991; McCarthy and Ellery, 1995). The Okavango Delta currently represents the terminal depository for the Okavango River system which drains from central Angola. The Okavango River degenerates into a series of anastomosing channels on the fan

surface which are bordered by extensive permanent fresh water swamps (6,000 km^2) in the proximal reaches of the fan (McCarthy et al., 1991). Seasonal flooding inundates a further 6,000 to 12,000 km^2 in the distal reaches (McCarthy and Ellery, 1995). The Okavango River transports sediments to the fan and the annual inflow of sediments amount to approximately 570,000 tons per annum (McCarthy and Ellery, 1998; McCarthy et al., 2002). Some 65% of the sediment consists of dissolved chemical matter and 35% is clastic, mainly bedload sands. To the sediment inflow is added another 250,000 tons of aerosols that are annually deposited over the delta (Garstang et al., 1998).

Evapotranspiration from the swamps exceeds precipitation by a factor of three and ~96% of the annual discharge is lost to the atmosphere (Dincer et al., 1981). Whereas the climate in the headwater region is subtropical and humid with annual precipitation of up to 1300 mm, it is semi-arid in Botswana with precipitation amounting to only 450 mm/year in the delta (Milzow et al., 2009). These conditions cause several of the small islands within the permanent swamps of the delta to accumulate sodium carbonate salts (trona) along the margins of the islands. The process responsible for the enrichment of dissolved solids (e.g. McCarthy et al., 1991) is evapotranspiration. Transpiration by trees and evaporation from salt pans on the islands cause drawdown of the water table. Swamp water (fresh water) enters the groundwater regime and flows toward the central depression becoming progressively enriched in solutes (i.e., calcite and SiO_2) owing to the selective removal of water to transpiring vegetation. Evaporation from the capillary zone in the area around the pans causes trona precipitation at the surface. Groundwater enters the pans by seepage, where strong evaporative

concentrations occur, producing dense brines which may percolate into the subsurface, displacing less-saline groundwater (McCarthy et al., 1991).

Continual movement and differential tilting along the faults in the lower Okavango Delta has caused changes in drainage pattern sedimentation within the distal regions of the delta. According to Campbell et al. (2006), the waxing and waning of the river systems has resulted in the inter-fingering of clay-rich sands and silts with fine-to-medium grained sand units. Near the distal ends of the delta, the mix of fluvial and deltaic Kalahari sediments has resulted in stacked freshwater aquifers in lensoid fine-to-medium grained sand units separated by clay-rich sands and silts above a brackish to saline "basement" aquifer. The transition zone from fresh to brackish and saline groundwater is generally of limited thickness, occurring over an interval of 2 m to (exceptionally) 10 m. An exception would be the Thamalakane aquifer located in between the Kunyere Fault and the Thamalakane Fault near the town of Maun. This freshwater aquifer is over ~15 km long and up to 2 km wide with a maximum thickness of ~80 m (Campbell et al., 2006).

2.2.1 Okavango Basin Evolution

Modie (2000) summarizes the basin evolution of Ghanzi-Chobe Belt. The Kgwebe Formation represents the earliest stage of basin development which has been dated 1106 +/- 2 Ma in age (Mesoproterozoic). The Kgwebe Formation formed from a collision-related extensional collapse associated with collision along the Namaqua-Natal Belt (Kampunzu et al, 1998). The Namaqua-Natal Belt extends from the west coast of South Africa eastward into Namibia. The extensional tectonics led to intracontinental

rifting and subsequent bimodal volcanism, depositing the metavolcanic rocks that compose the Kgwebe Formation. Sedimentation within the intercratonic rift was also occurring during this time, forming the overlying Neoproterozic Ghanzi Group sequence. The medisedimentary Ghanzi Group displays steep northeast trending foliation and shallow plunging fold axes (Schwartz and Akanyang, 1994; Akanyang, 1997) resulting from tectonic deformation during the Pan African Damaran Orogeny approximately 650 Ma ago. The Paleozoic to mid-Mesozoic Karoo Supergroup unconformably overlies the basement rocks. Jurassic post-Karoo basalts cover large areas of the bedrock. The 178 – 181 Ma (Jurassic) post-Karoo dolerite dike swarm formed a 110 km-wide and ~2000 km-long west-northwest-east-southeast trending swarm. It is believed that the dikes were emplaced in a pre-existing zone of weakness in the basement either by mantle processes or stress-release between adjacent rigid plates (Modisi, 2000; Aubourg et al., 2008). Cenozoic deposits consisting of fluviatile fine sand and clay of the Okavango alluvial fan (Thomas and Shaw, 1991) cover the entire area of the ORZ. Aeolian Kalahari beds that have been reworked by fluvial processes in the Okavango alluvial fan cover the surrounding areas (Modisi, 2000).

Initiation of current rifting processes in the ORZ are unknown; however, paleoenvironmental reconstruction from sediments collected in Lake Ngami suggests that feeder rivers promoted extensive flow beyond the Thamalakane and Kunyere faults circa and beyond 120 Ka into the Makgadikgadi pans. Between 120 Ka and ~ 40 Ka, neotectonic activity resulted in uplift along the Zimbabwe-Kalahari axis and displacement along the northeast-southwest trending faults resulting in the impoundment of the proto-Okavango, Kwando, and the upper Zambezi rivers and the development of

the proto-Makgadikgadi, Ngami, and Mababe sub-basins (Cooke 1984; Thomas and Shaw, 1991; Moore and Larkin, 2001; Ringrose et al., 2005) suggesting that rifting may have been initiated about 40 Ka.

Recent paleoenvironmental studies performed by Gamrod (2009) from the Mababe depression suggest that neotectonic activity may have been initiated between ~40 Ka and 27 Ka. Dates obtained from sediments sampled from the Mababe depression show a change in the sediment and hydrologic regime of the depression during this time. The change in the sedimentation record is attributed to possible movement along the Linyanti Fault. Prior to tectonic activity, the entire discharge of the Kwando River likely flowed into the Mababe depression via the Savuti channel and the Tsatsara gap (Grove, 1969; Shaw1985). Uplift along the Linyanti Fault diverted flow of the Kwando River to the Zambezi River and away from the Mababe depression. Rifting processes also resulted in the impoundment of the Okavango River and initiation of the formation and development of the delta to its current form.

CHAPTER III

METHODOLOGY

3.1 Electrical Resistivity Tomography (ERT)

Electrical resistivity tomography (ERT) measures the potential difference at points on the Earth's surface produced by direct or low frequency alternating current flow injected into the ground. The resulting measured voltage is used to calculate the ground's resistance to current flow. Resistivity (or its reciprocal, conductivity) is dependent upon porosity, fluid saturation, and ions in solution within the pore spaces of a medium (e.g., Jones, 1992). An increase in these factors allows for greater electrical current flow through a medium (i.e., the medium is "conductive"). A decrease in these factors causes the medium to be resistant to current flow (i.e., the medium is "resistive"). Normal faults are usually observed on ERT profiles as sharp lateral resistivity contrasts (e.g., Suzuki et al., 2000; Caputo et al., 2003; Diaferia et al., 2006) caused by the juxtaposition of different sediment layers and/or by different hydrological conditions on either side of the fault.

We acquired four profiles using AGI's SuperSting R8 Resistivity/IP System across several of the faults bounding the southern grabens of the ORZ. Profile 1 (Figure 3A) traversed the southwestern boundary of Lake Ngami and was ~ 9 km long. We used a dipole-dipole array with 56 electrodes and 10-m spacing between each electrode along

each spread. Each spread was 550 m in length with overlap of spreads occurring every half spread (275 m). Profiles 2 and 3 were both 80 km and 90 km north of Lake Ngami respectively (Figure 3C). Both profiles were ~2.0 km long and were acquired using the same dipole-dipole array with 42 electrodes and 10-m spacing for each spread. The spreads were 410 m in length with spread overlaps every half spread (205 m). Profile 4 (Figure 3D) spanned a length of almost 10 km across the Mababe depression. A dipole-dipole array was used with 72 electrodes and 10-m spacing between each electrode per spread. The 710-m spreads overlapped every half spread (355 m).

The measured apparent resistivity values were inverted to obtain a model of true subsurface resistivity using AGI's EarthImager 2D software. Our criteria for inversion included robust inversion and an L2- Norm method available in this program. An RMS error of <10% was our goal. Each inverted section produced from EarthImager was imported into Geosoft's Oasis Montaj software to create resistivity images for each of the profiles.

3.2. Magnetotelluric (MT) Method

Active structures in the Earth's crust are often conduits for fluids (Park and Wernicke, 2003). One of the most sensitive indicators of these fluids is electrical conductivity. The magnetotelluric method simultaneously measures the magnitude of the Earth's natural horizontal electric and magnetic field components over a wide range of frequencies which are then converted and used to compute the resistivity of a material. The electromagnetic energy comes from natural transient sources such as solar wind-induced flow of charged particles in the ionosphere and distance thunderstorm activity.

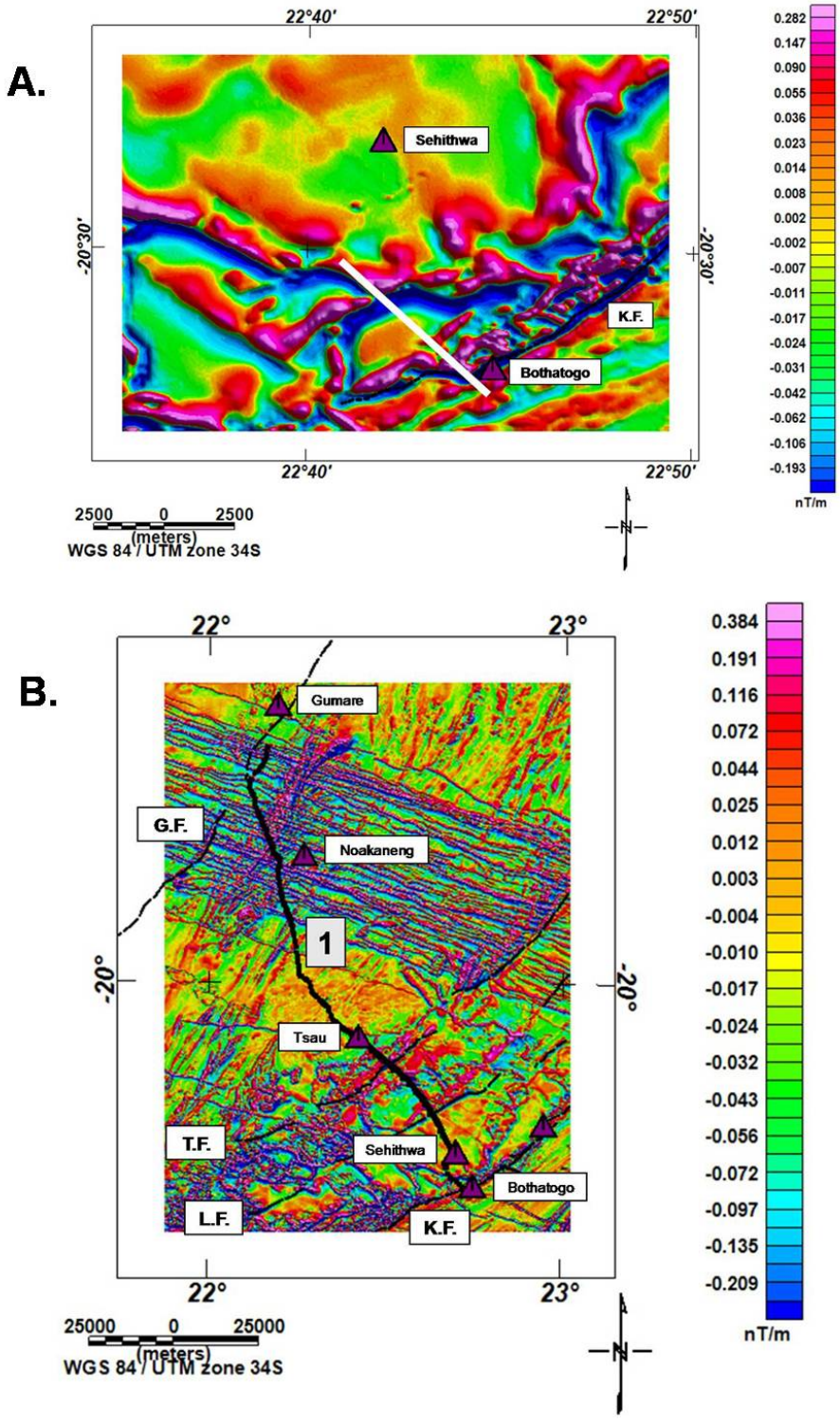

Figure 3. Vertical derivative aeromagnetic anomaly maps. A.) Electrical Resistivity Tomography (ERT) station locations for Profile 1 (white line). B.) Magnetotelluric (MT) and magnetic station locations for Profile 1. G.F. = Gumare Fault, T.F. = Tsau Fault, L.F. = Lecha Fault, K.F. = Kunyere Fault.

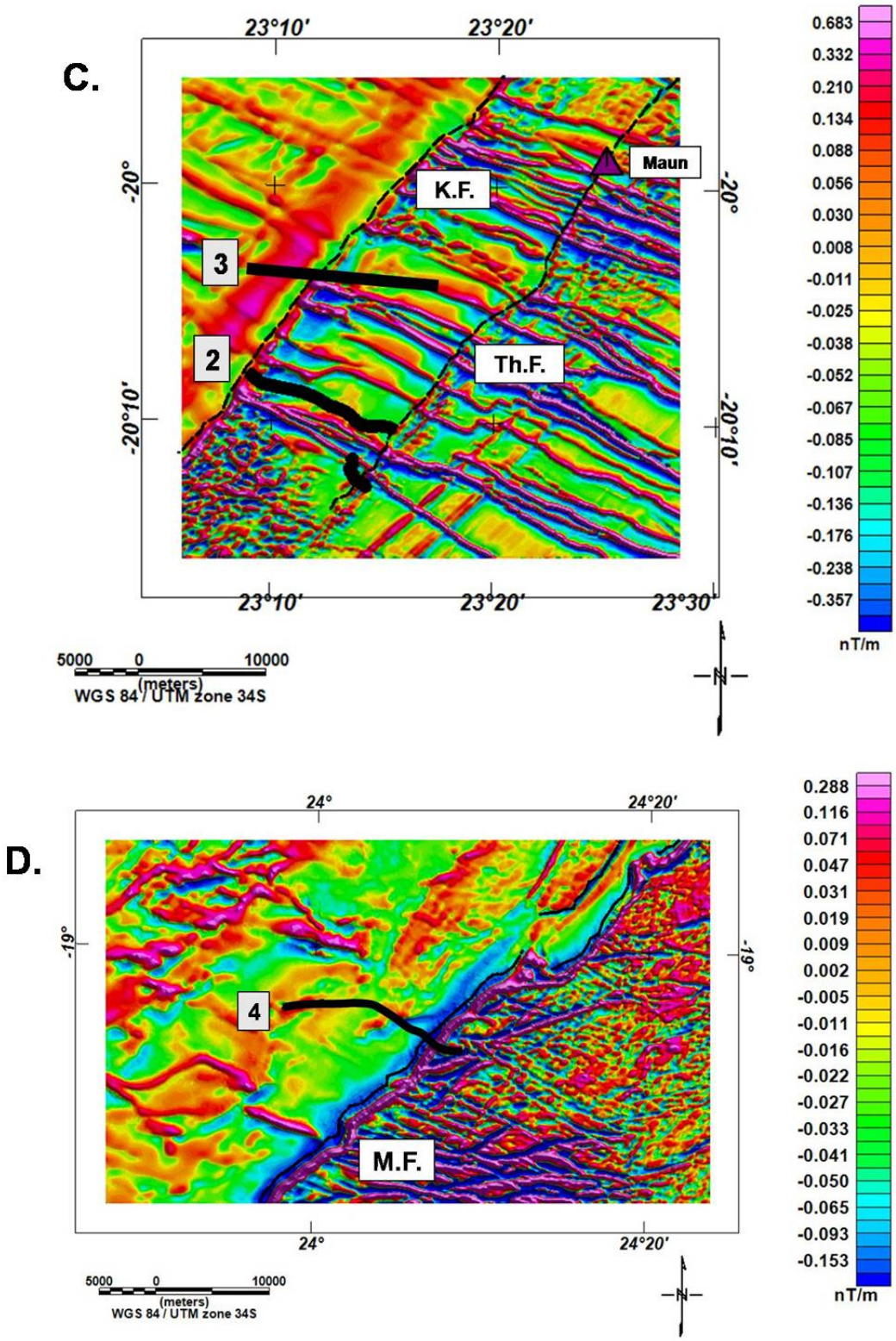

Figure 3 (cont). Vertical derivative aeromagnetic anomaly maps. C.) ERT, MT, and magnetic station locations for Profile 2 and Profile 3. D.) ERT, MT, and magnetic station locations for Profile 4. K.F. = Kunyere Fault, Th.F. = Thamalakane Fault, and M.F. = Mababe Fault.

As the electromagnetic fields come in contact with the Earth's surface, part of the energy is refracted into the ground and induces time-varying telluric currents (natural alternating electric fields that flow within the earth). When these currents come in contact with a conductive material, the currents generate a secondary field measured by the MT system. The electromagnetic energy source for our surveys came from distant thunderstorms. Since fluid transport within rocks opens pores and cracks which in turn increases the mobility of solutes such as salts, calcite, or quartz within the pores (Ritter et al., 2005), the MT method can detect vertical conductive zones which are characteristic of active faults. Faults are often less resistive than their host rocks because of increased porosity, fluid flow, and/or the presence of alteration material within the fault zone (Tournerie and Chouteau, 2001). Certain types of mineralization, such as graphite precipitation, can lead to conductive old and inactive faults; however, active tectonic activity is generally required to maintain the interconnectivity of the pore space in the rock (Park and Wernicke, 2003).

Four MT profiles were acquired across the faults bounding the ORZ. Profile 1 (Figure 3B) extended 140 km across the southern part of the rift while Profile 2 and Profile 3 (Figure 3C) near Maun were 15 and 22 km long respectively. Profile 4 (Figure 3D) extended across the Mababe depression for ~9.2 km. We used Geometric's Stratagem EH4 instrumentation which consisted of metal stakes (electrodes) and induction magnetic coils to measure the magnitude of the Earth's horizontal electric and magnetic field components respectively. Measurements were collected within three frequency ranges: 10 – 1000 Hz, 500 Hz – 3 KHz, and 750 Hz – 9.6 KHz. The first two frequency ranges were natural while the third frequency range was measured by injecting

current into the ground via a transmitter. Our dipole length was 50 m. Station spacing ranged from 50 m to 5 km, depending on the proximity of a fault (i.e., stations were closely spaced when crossing a fault).

The data was processed using GEOSYSTEM's WinGLink program. Methods similar to Tournerie and Chouteau (2002), Park and Wernicke (2003), and Whaler and Houtot (2006) were utilized for the processing of our data. Whaler and Houtot (2006) suggest that subsurface structures only emerge when the electromagnetic field components are measured in, or rotated into, coordinates defined by the strike direction and perpendicular to it. This dilemma occurs because currents parallel to structure only induce magnetic fields perpendicular to it (transverse electric "TE" mode) and currents perpendicular to strike only induce parallel magnetic fields (transverse magnetic "TM" mode). Thus, the diagonal elements of the impedance tensor vanish. To ensure that their structures were imaged correctly, Whaler and Houtot (2006) determined the best 2D approximation of a 3D structure by rotating the impedance tensor such that its diagonal elements were a minimum, on a site-by-site and period-by-period basis. Tournerie and Chouteau (2002) and Park and Wernicke (2003) performed similar steps by first identifying regional geoelectrical strike and then rotating impedance tensors and magnetic transfer functions to regional strike. Prior to inversion, the electromagnetic field components for each station were rotated parallel to regional strike. For our data, we used 060^{o} for Profiles 1, 2, and 3. Profile 4 sounding curves were rotated to 040^{o}. TE and TM can be set for either the north-south direction (xy) or the east-west direction (yx). For our data, the WinGLink program set TE equal to xy and TM equal to yx based off the data we collected.

1.) TE Impedance Tenor: $\rho = \frac{1}{5f}\left(\frac{Ey}{Hx}\right)^2$

2.) TM Impedance Tenor: $\rho = \frac{1}{5f}\left(\frac{Ex}{Hy}\right)^2$

Where ρ is resistivity, *f* is frequency, *Ex* and *Ey* are the horizontal components of the electric field, and *Hx* and *Hy* are the horizontal components of the magnetic field.

For each inversion, the smoothed apparent resistivity curves were used. Both TE and TM impedance modes were utilized for the inversion process and depths were constrained based on the maximum penetration depths for each station within a profile. Error floors ranging from 20% to 30% were used during the inversion process in order to lower the root-mean-square (RMS) error and to reduce the influence of data values with unrealistically low error estimates (Park and Wernicke, 2003). We chose an RMS error of 3% for our best fitting 2D models. We kept the color scheme for the resistivity values of our models "low" in order to separate the conductivity of the faults from the extremely conductive environment of the grabens. Due to poor data quality, MT Profiles 3 and 4 will not be presented.

3.3. Total Field Magnetic Surveys

Both ground and aeromagnetic surveys were used for our study. For our ground surveys (Figure 3B – 3D), we used GEM System's proton precession magnetometer. Over 150 km of ground magnetic data were acquired for Profile 1 using 100-m spacing between each station. Data was collected for Profiles 2 and 3 every 100 m and 250 m respectively. Profile 2 ranged over 18 km in length and Profile 3 extended over 20 km in

length. The displacement along Profile 2 on Figure 3C is due to a change in location during our acquisition process. Profile 4 over the Mababe depression was ~20 km long and stations were spaced every 10 m. Closer spacing was implemented when crossing a fault.

The aeromagnetic data used in this study, also used by Kinabo et al. (2007; 2008), was acquired in 1996 and has been provided by the Geological Survey of Botswana. The flight elevation for the aeromagnetic data was 80 m along north-south lines with spacing of 250 m. The tie lines were east-west and spaced 1.25 km apart. The international geomagnetic reference field was removed and the data were gridded in Geosoft's Oasis Montaj program with a grid cell size of 62.5 m. Derivative filters were applied to the residual total field magnetic data in order to highlight the main structural features of the area which include faults, dikes, and folds.

2D magnetic models were created from our ground surveys using NGA's GM-SYS modeling software. Total magnetic field, inclination, and declination parameters were input into the software in order to correctly model the data over the ORZ. The basement cut by current faulting is interpreted to be the metavolcanic rocks of the Kgewbe Formation and the metasediments of the Ghanzi Group. Therefore, we used susceptibility values ranging from 4.3×10^{-5} to 2.0×10^{-4} SI to represent the basalts, metavolcanics, and metasediments that compose the basement material.

3.4. Gravity

Two gravity profiles were used for our study (Figure 4). The data for Profile 1(Figure 4A) was provided to us by the Geological Survey of Botswana. The profile

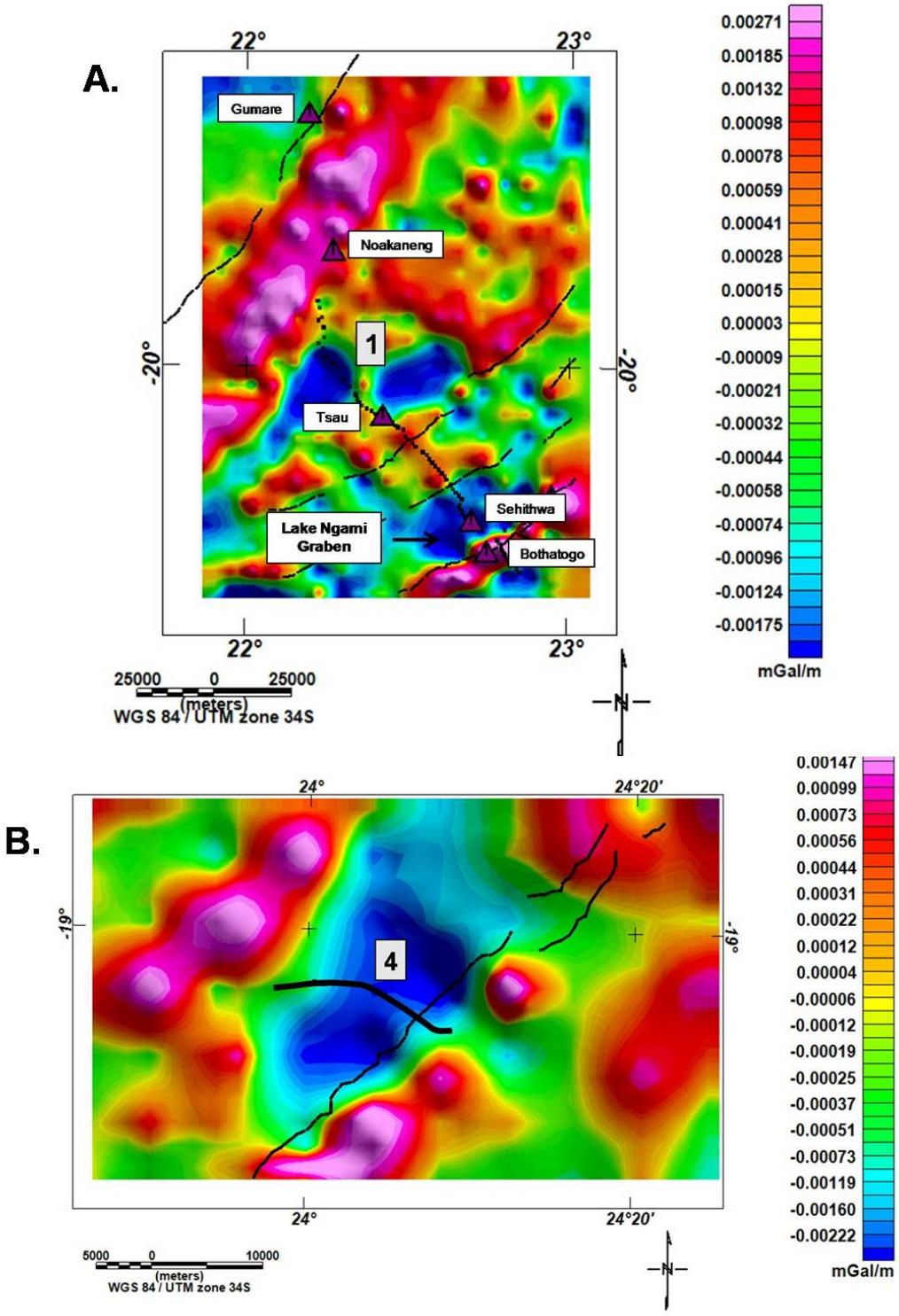

Figure 4. Vertical derivative gravity anomaly maps displaying station locations for A.) Profile 1 through the Lake Ngami graben and B.) Profile 4 through the Mababe depression. Dashed lines delineate the location of the faults in relation to the grabens. Triangles represent the locations of towns and villages.

spanned over 120 km in length along a stretch of highway between the village of Bothatogo and the town of Gumare. A reading was taken every ~200 m. The second profile was Profile 4 (Figure 4B) which was acquired in the Mababe depression using a Scintrex CG-5 autograv gravity meter. Readings were collected every 100 m. For the Mababe profile, relative elevation was determined using a total station tied to the elevation of the absolute gravity station at the Maun airport. Tidal, free air, and Bouguer corrections were applied to the data set using 2.67 g/cm^3 reduction density.

The gravity data presented in Figure 4 was acquired in 1999 on a 7.5 km grid with an acquisition accuracy of 0.2 mGal. The data was made available for our study by the Geological Survey of Botswana. Tidal, free air and Bouguer corrections were applied to the data and the data was gridded with a grid cell size of 1.84 km using Geosoft's Oasis Montaj program.

2D gravity models were constructed using NGA's GM-SYS modeling software to determine the subsurface structure of the basins and sediment thickness. The main parameters used for the models were sediment density and the density associated with basement rocks. Depths obtained from Euler deconvolution solutions (Thompson, 1982) and results from Kinabo et al. (2007;2008) were used as estimates for sediment fill. Density values were obtained from Telford et al. (1990) based on the lithologies of the rocks and sediments that compose the rift.

CHAPTER IV

RESULTS

4.1. Electrical Resistivity

For Profile 1 (Figure 5A), we displayed only the first 4200 m. The final 5000 m was acquired over the graben and showed minimal changes in the geoelectric sections. Profile 1 across the Kunyere Fault near Lake Ngami suggests a depth of penetration of ~100 m. Higher resistivity values characterize the SE section of the profile over the basement. Three geoelectric units are observed: a top unit occurs at a depth of 10 to 20 m and consists of resistivity values ranging from 660 – 1300 Ohm.m. This resistive layer extends for ~1500 m along the profile from Bothatogo Village before transitioning into less resistive material within the graben, which is predominantly composed of low resistivity values ranging from 0.9 – 30 Ohm.m. The upper resistive layer is underlain by a second layer of less resistive material ranging from 40 – 300 Ohm.m. A third more resistive geoelectric unit near the bottom of the profile has values ranging from ~400 – 5000+ Ohm.m. According to the location of Profile 1 on the regional aeromagnetic map of the area, the Kunyere Fault near Lake Ngami is located between 2550 and 3100 m (arrows) on the profile. Note that the area containing the fault shows a laterally discontinuous geoelectric unit of resistive rock juxtaposed against conductive sediments

delineated by sharp boundaries and is located after the exposed fault scarp.

Profile 2, located 80 km northeast of Lake Ngami, is composed of two geoelectric units: a thin resistive top layer similar to Profile 1 ranging from 300 – 5000+ Ohm.m underlain by a second less resistive layer 0.9 – 200 Ohm.m (Figure 5B). The resistive layer continues for ~1200 m to the northwest before disappearing and then reappearing for ~200 m near the beginning of the profile. The second less resistive layer is fairly consistent except for an area between 1000 and 1400 m which exhibits discontinuity where resistive material is inter-mixed with conductive sediments. The Thamalakane Fault is located approximately 1300 m from the southeast.

The presence of a resistive layer capping the surface of the profile is less apparent on Profile 3 (Figure 5C), which is located 10 km northeast of Profile 2. However, the resistive top layer can be seen for the last 200 m near the end of the profile which displays an area of sharp resistivity contrasts. The Kunyere Fault near Maun is located within the discontinuous zone (approximately 2500 m from the west). The remainder of the profile is predominantly a mixture of conductive and resistive (0.9 – 700 Ohm.m) material before reaching the graben, which is composed of conductive sediments ranging from 0.9 – 80 Ohm.m.

Profile 4 in the Mababe depression (Figure 5D) parallels Profile 3 by displaying a similar two-layered geoelectric model: the first layer being the characteristic thin resistive zone near the surface ranging from ~20 – 80 Ohm.m and the second layer at depth consisting of less resistive sediments measuring 0.2 – 10 Ohm.m. The thin resistive top layer is most apparent in the southeast near the end of the profile and is especially resistive between 7000 and 8200 m. This thin resistive zone exists throughout the entire

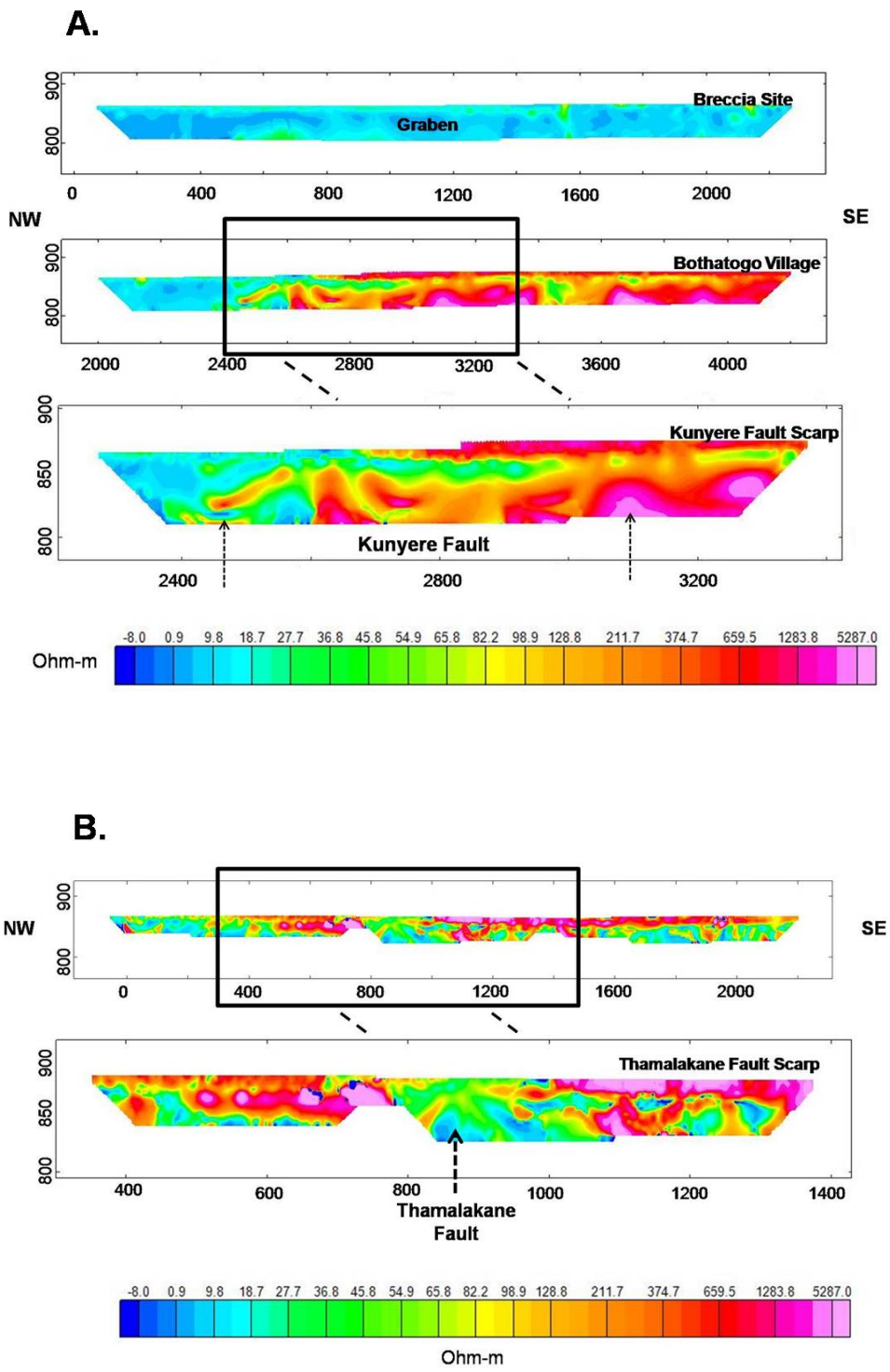

Figure 5. 2D resistivity sections for A.) Profile 1 across the Kunyere Fault and B.) Profile 2 across the Thamalakane Fault. Arrows indicate fault locations. See Figure 3 for profile locations on the vertical derivative aeromagnetic anomaly map.

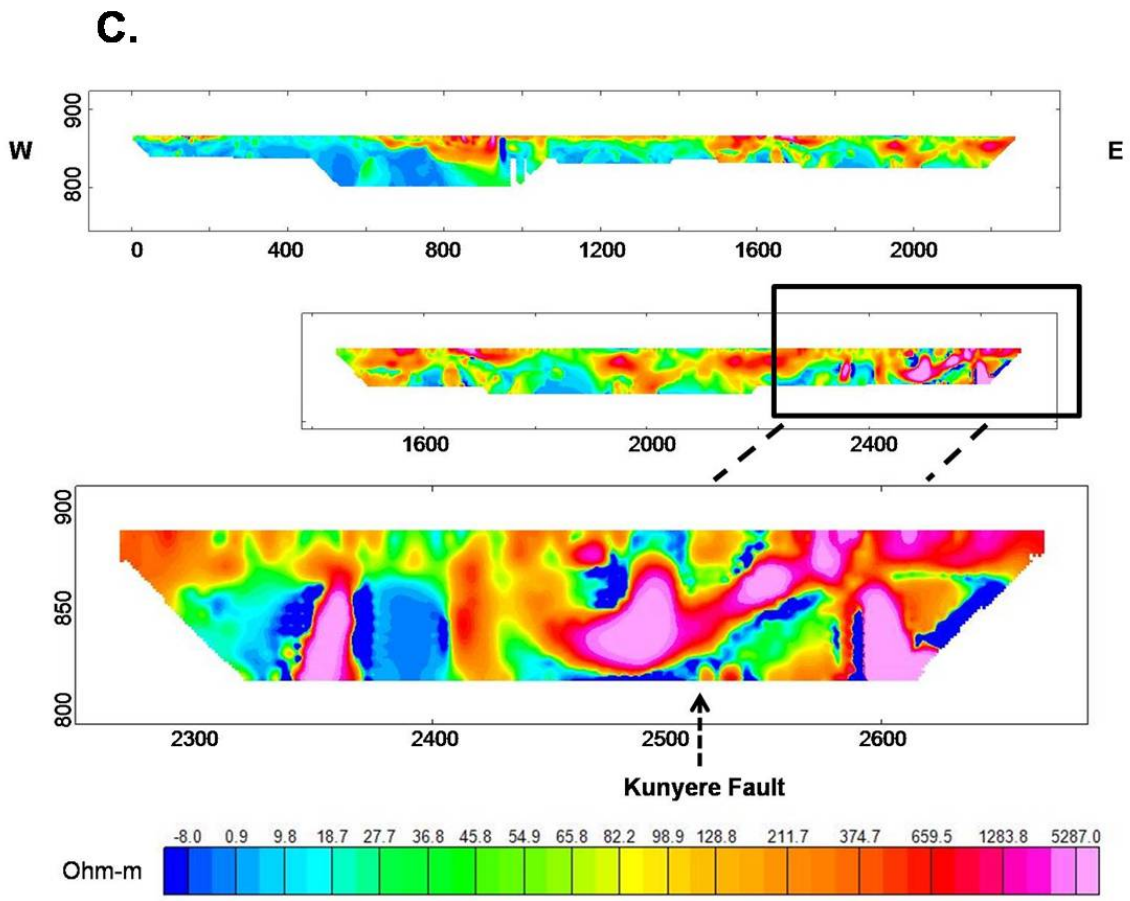

Figure 5 (cont). 2D resistivity section for C.) Profile 3 across the Kunyere Fault. Arrow indicates fault location. See Figure 3 for profile location on the vertical derivative aeromagnetic anomaly map.

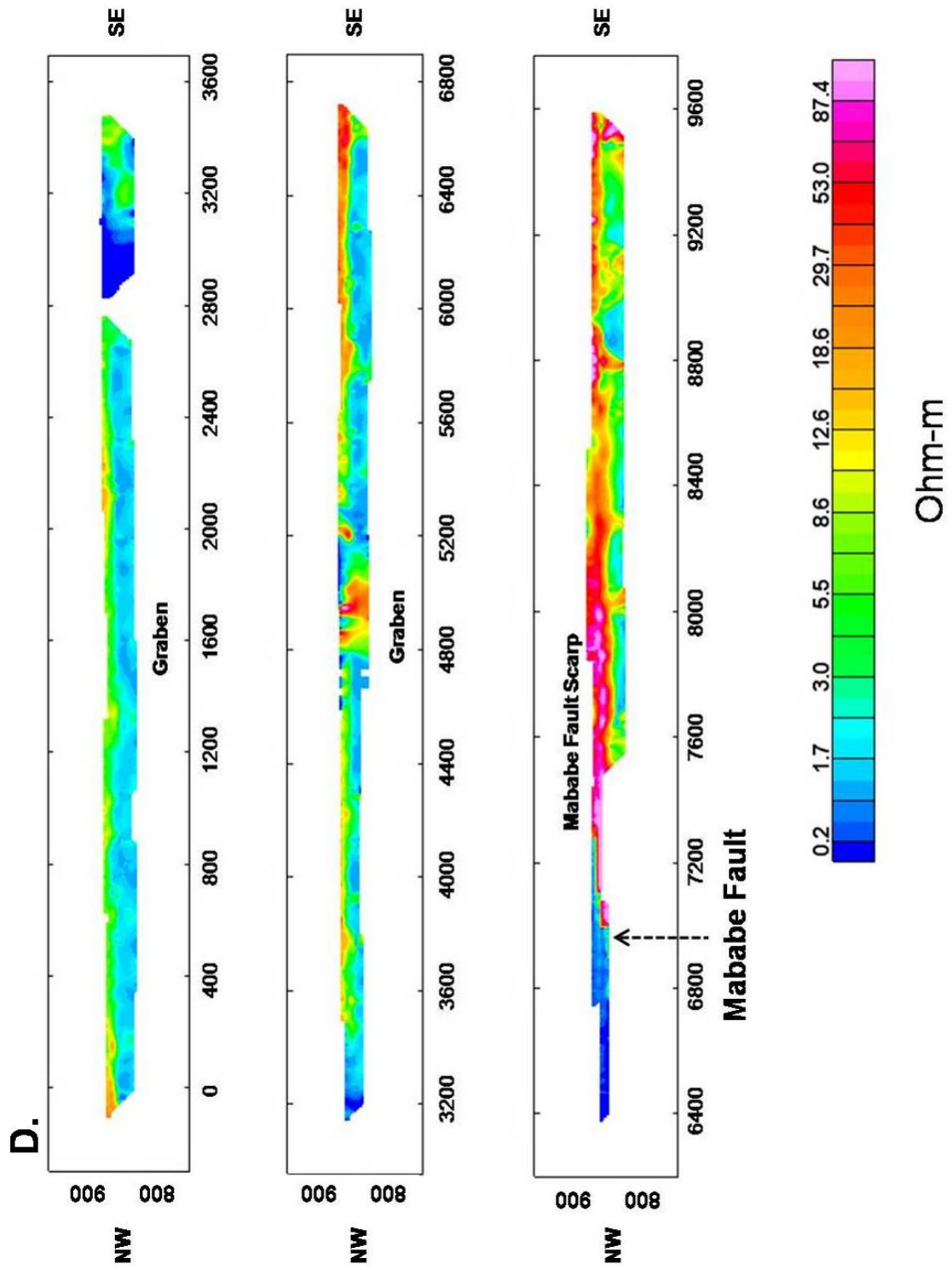

Figure 5 (cont). 2D resistivity sections for D) Profile 4 across the Mababe Fault. Arrow indicates fault location. See Figure 3 for profile location on the vertical derivative aeromagnetic anomaly map.

profile, even though the resistivity of the layer decreases in the graben which contains sediments ranging from 0.2 – 50 Ohm.m. The location of the profile on regional aeromagnetic maps places the Mababe Fault between 6800 and 7200 m.

4.2 MT

Our MT results are presented as 2D inverted cross-sections. Their accompanying mesh inversions are located in the Appendix. Penetration depths for Profile 1 (Figure 6 A3) reached as deep as 1700 m below the surface along the footwall of the Kunyere Fault; however, only the top 400 m are shown for our complete 2D MT inversion model due to the highly conductive environment and lack of penetration within the graben. The model displays three distinct vertical areas of high conductivity ranging from 6 – 12 Ohm.m (from northwest to southeast) below stations 59 – 63, 49 – 48, and 37 – 31. According to the location of the profile on the regional aeromagnetic map, stations 49 – 48 cross the Tsau Fault and stations 37 – 35 cross the Lecha Fault. The cause of the third conductive zone (stations 059 – 063) is unknown. However, a ternary map of the area near the conductive anomaly (Figure 9G) shows a structure within the basement that may be responsible for the low resistivity values associated with this zone. Along the profile, the three conductive zones are separated by sediments of higher resistivity. The highest values are located near the town of Gumare at the beginning of the profile and at the end of the profile near Bothatogo Village within the basement rocks.

In order to further investigate the detailed structure of the Tsau and Lecha faults within the subsurface, a second inversion near the faults was performed for Profile 1 (Figure 6B). It is apparent from the inversion that the Lecha Fault has a broader area of

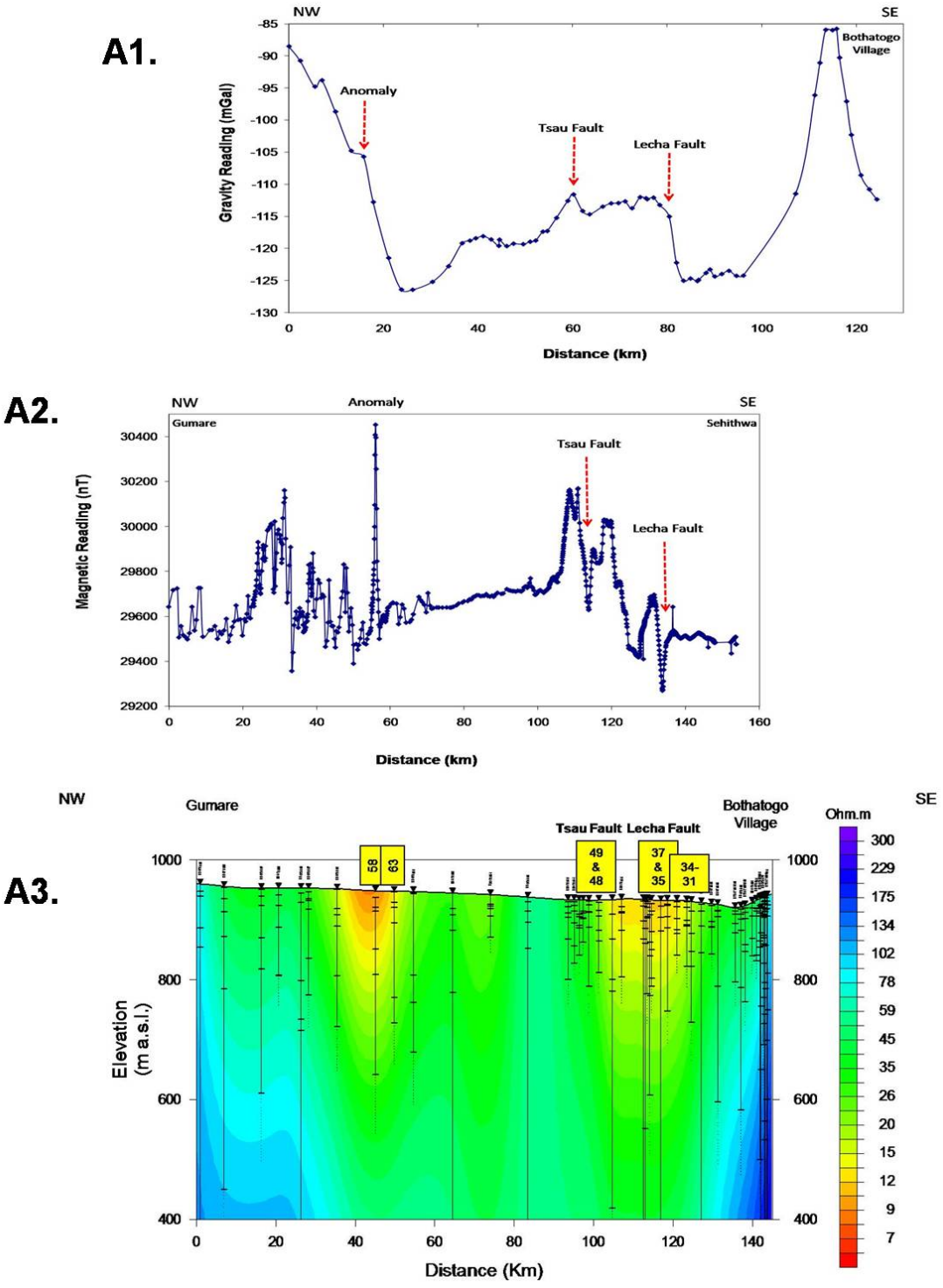

Figure 6. Gravity profile (A1), magnetic profile (A2), and the MT inverted cross-section model (A3) for Profile1. Fault locations are indicated by arrows on the gravity and magnetic profile. See Figure 3 for profile locations on the vertical derivative aeromagnetic anomaly map and Figure 4 for profile locations on the vertical derivative gravity anomaly map.

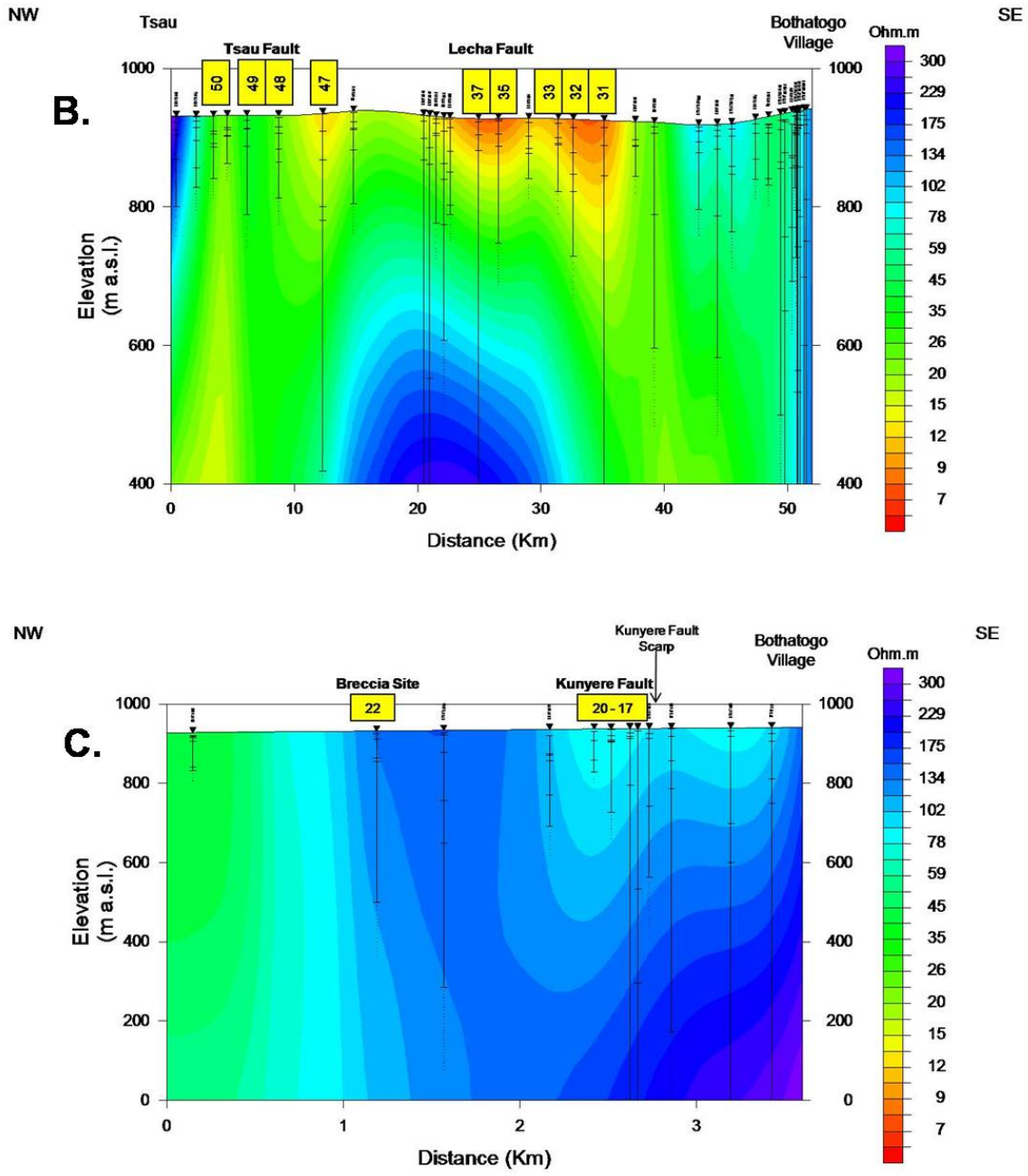

Figure 6 (cont). Figure 6B and 6C are enlarged areas of the Profile 1 MT model to further investigate the conductive behavior of the Tsau, Lecha (6B), and Kunyere (6C) faults. See Figure 3 for profile location on the vertical derivative aeromagnetic anomaly map.

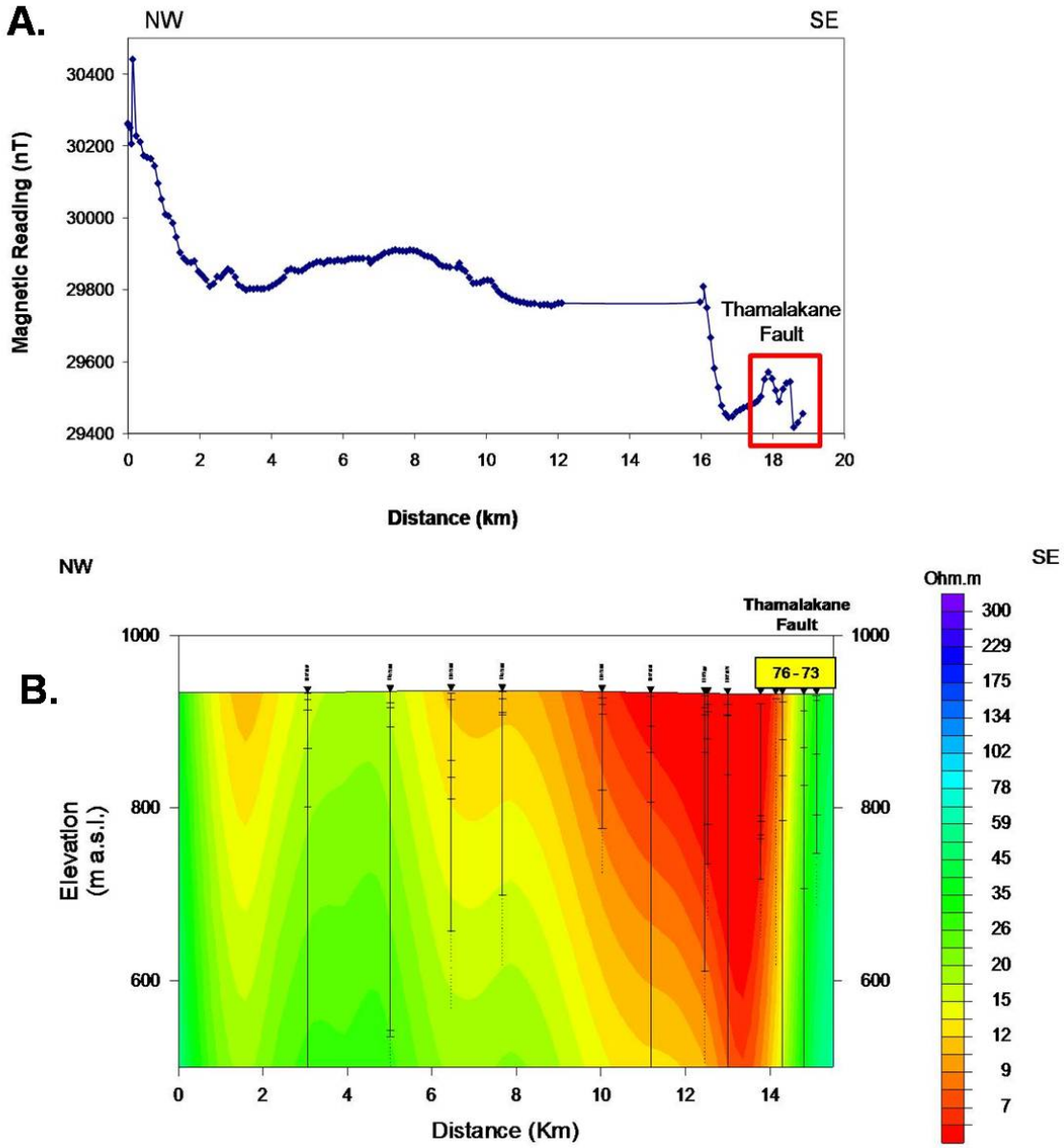

Figure 7. Magnetic profile (A) and the MT inverted cross-section model (B) for Profile 2 across the Thamalakane Fault. The location of the Thamalakane Fault is delineated by a red rectangle on the magnetic data. See Figure 3 for profile location on the vertical derivative aeromagnetic anomaly map.

conductivity than the Tsau Fault. Note the second area of high conductivity southeast of the Lecha Fault beneath stations 33 – 31 ranging from 7 – 12 Ohm.m. The Tsau Fault appears to have a narrow area of conductivity expressed by anomalies ranging from 6 – 9 Ohm.m on the mesh model (Appendix A2) northwest and southeast of the fault. According to the cross-section (Figure 6B), the anomalies near the Lecha Fault reach a depth of ~150 m below the surface while the Tsau Fault anomalies reach a much shallower depth of ~50 m below the surface.

To investigate the character and geometry of the Kunyere Fault near Lake Ngami, we present a third inversion of Profile 1 (Figure 6C). Regional aeromagnetic maps place the Kunyere Fault between stations 20 – 17. The model displays an area of resistive material from Bothatogo Village to station 22. Note how the resistive anomaly continues well beyond the fault scarp (footwall) and into the graben. Also, notice how the Kunyere Fault is not delineated by a vertical conductive feature. Instead, there is a very sharp boundary between the resistive material associated with the footwall and the conductive sediments within the graben.

For Profile 2 (Figure 7B), the deepest depth of penetration reached close to 700 m below the surface; however, we displayed only the top 400 m. The 2D MT mesh inversion model (Appendix A4) and cross section both show one well-defined area of high conductivity (6 – 9 Ohm.m) below stations 76 – 73 that reaches a depth of ~250 – 300 m below the surface. The location of the profile on the regional aeromagnetic map near Maun suggests that the Thamalakane Fault is crossed between these stations.

4.3 Total Field Magnetic Surveys

Along Profile 1 (Figure 6 A2), the Tsau and Lecha faults are depicted as large magnetic "spikes" within the data set. According to the location of Profile 1 on regional aeromagnetic maps of the area, the profile intersects the Tsau and Lecha faults between 113 and 114 km respectively. The Tsau and Lecha magnetic spikes occur in the same locality as the conductive anomalies representing these faults on MT Profile 1. The very large spike between 55 – 57 km is an unknown anomaly; however, the large spike is located within the same vicinity as the anomalous zone of low conductivity on MT Profile 1 (stations 59 – 63).

The same characteristic spike associated with the Tsau and Lecha faults within our area of interest can also be seen on Profile 2 (Figure 7A). The Thamalakane Fault (delineated by the red rectangle) is located at the end of the profile between 18 – 19 km according to the placement of the profile on the regional aeromagnetic map of the area. The location of both the magnetic and MT profiles on the regional aeromagnetic map place the Thamalakane Fault within the same locality.

The location of the Kunyere Fault near Maun for Profile 3 (Figure 8A) is not exact. Latitude and longitude coordinates were not collected for this profile; however, MT stations containing latitude and longitude coordinates were collected in this area. Both ground magnetic and MT acquisition profiles were approximately collected over the same area. The possible fault location is based on the location of the MT stations and vertical derivative regional aeromagnetic maps of our area of interest. The magnetic spike signature is not as apparent for the Kunyere Fault as seen by the Tsau, Lecha, and Thamalakane faults; however, a magnetic high is visible before transitioning into a magnetic low, which is characteristic of the Tsau, Lecha, and Thamalakane faults.

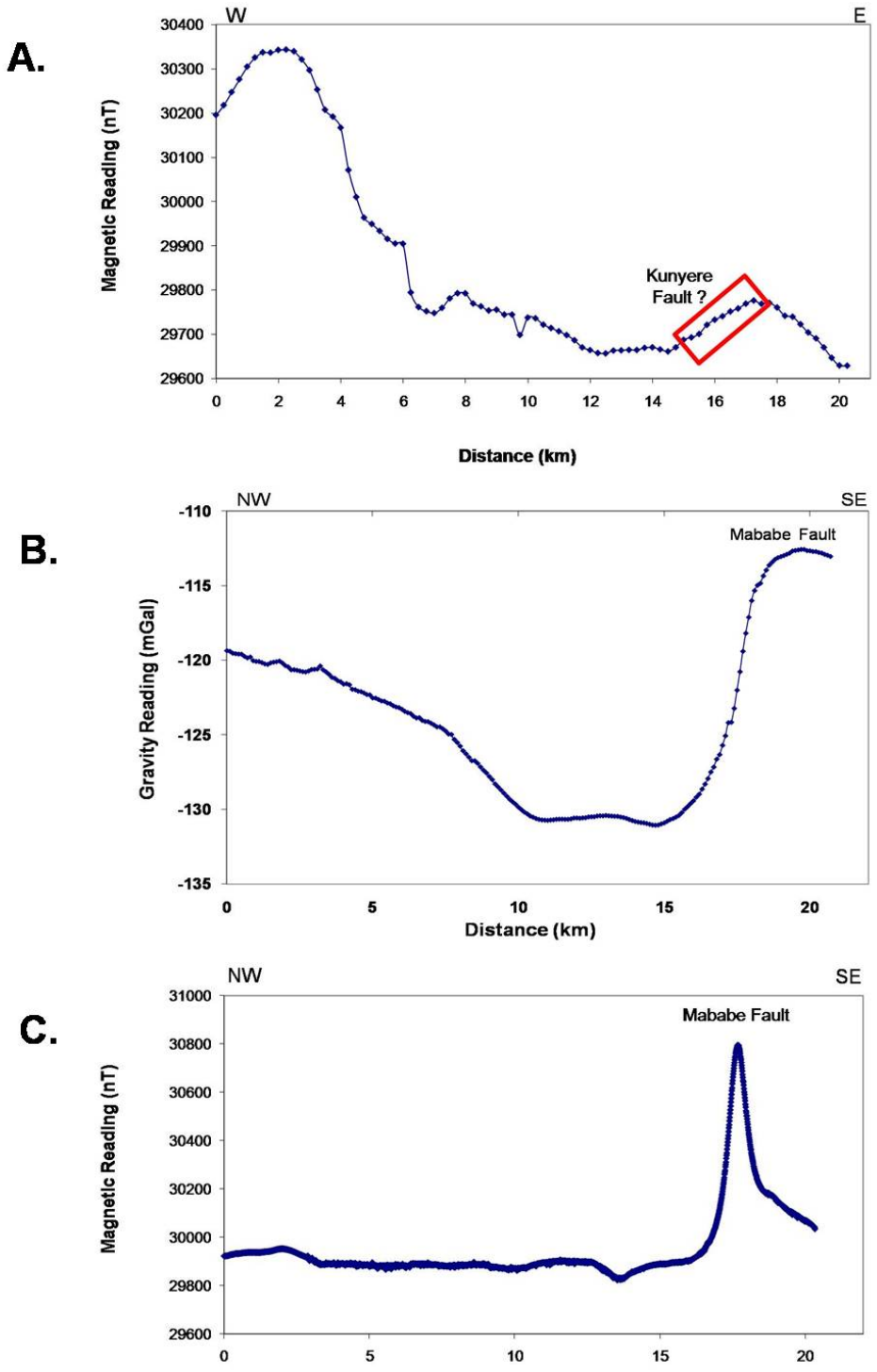

Figure 8. Gravity and magnetic profiles. A.) Profile 3 magnetic data across the Kunyere Fault. B.) Profile 4 gravity data across the Mababe depression. C.) Profile 4 magnetic data across the Mababe Fault. See Figure 3 for profile locations on the vertical derivative aeromagnetic anomaly map and Figure 4 for profile locations on the vertical derivative gravity anomaly map.

The Mababe fault along Profile 4 (Figure 8C) is represented as a very strong magnetic spike reading 30800 nT. Unlike the other faults within our area of interest, the Mababe fault is depicted as a positive anomaly where as the Tsau, Lecha, Thamalakane, and Kunyere faults are all characterized by negative anomalies.

4.4 Gravity

Two distinct lows are present on Profile 1, the first is located between 20 and 40 km and the second between 80 and 100 km (Figure 6 A1). Both lows can be easily seen on the vertical derivative gravity map as depressions (Figure 4A). The lows both have a gravity reading of ~ -127 mGals. Profile 4 (Figure 8B) depicts an 18 km-wide low that is also very distinct on the vertical derivative gravity map (Figure 4B).

CHAPTER V

DISCUSSION

Previous research conducted by Kinabo et al. (2007; 2008) has provided some understanding about specific characteristics associated with the five faults of interest within our investigation. Through our continued research over these faults, we aim to grasp a better understanding of their tectonic activity, fault zone architecture, magnetic characteristics, and the implication of these findings as they relate to fluid flow along the faults.

Several studies have used electrical geophysical techniques, in particular MT, to characterize the activity of faults. For example, in MT studies across several fault zones, Ritter et al (2005) were able to document that the conductivity structure of active faults were distinctly different from inactive faults. Active fault zones were characterized by a distinct fault zone conductor (FZC), while inactive zones tend to lack a FZC. For example, in the central segment of the San Andreas Fault, a zone of high conductivity extending to a depth of several kilometers and attributed to fluids within a highly fractured damage zone is associated with the seismogenic zone (creeping segments), whereas locked segments (e.g., the Carrizo segment) lacked the strong conducive signature (Mackie et al., 1997; Unsworth et al., 1997; Unsworth et al., 1999; Unsworth et al., 2000; Bedrosian et al., 2004; Unsworth and Bedrosian, 2004; Ritter et al., 2005).

These studies suggest the important role of fluids in fault activity and earthquake generation. The results of our study suggest that the major faults display different conductivity structures which we infer may be related to the activity of the faults.

5.1 Fault Activity

5.1.1. Tsau Fault and Lecha Fault

The Tsau and Lecha faults are well expressed on the aeromagnetic maps within the basement (Figure 3B) however; unlike the other faults of the ORZ (i.e. – Kunyere, Thamalakane and Mababe) which have well defined topographic scarps, these faults lack any surface expression leading to the suggestion that they are 1.) inactive, 2.) concealed by rapid sedimentation associated with Okavango alluvial fan deposits (i.e., sedimentation rates are higher than vertical movement of the faults), or 3.) they were reactivated but lack sufficient energy to rupture the surface (i.e., blind normal faults). The MT Profile 1 (Figure 6B) shows conductive anomalies that coincide with the surface location of the Tsau and Lecha faults. We interpret this fault zone conductivity anomaly to be related to the presence of fluids. Because of the high conductivity associated with the sediments within the graben, the MT profiles did not image the basement, hence the results only show conductive anomalies located within the sedimentary cover. We infer from this observation that both the Tsau and Lecha faults have propagated into the shallow sediments, at least to a depth of 30 m, suggesting continued activity of the faults.

The conductive anomalies surrounding the faults on Figure 6B may suggest multiple faulting or splays from the Tsau and Lecha faults, which is consistent with Kinabo et al. (2008) explanation of fault-plane propagation. As the leading edge of the

main propagating fault plane approaches the hard-rock sediment interface, strain resulting from extensional processes is accommodated, causing the fault plane to splay into different fault segments which rupture at the surface. These splays are depicted on the MT models as separate zones of conductivity near the location of the faults.

5.1.2 Kunyere Fault

In contrast to the Tsau and Lecha faults, the Kunyere Fault near Lake Ngami on MT Profile 1 lacks the FZC signature characteristic of active faults (Figure 6C). This observation is consistent with Kinabo et al. (2008) who suggest that tectonic activity is waning along the southwestern segment of the Kunyere Fault as strain is being transferred to the younger more active Thamalakane Fault in the northeast. The Kunyere Fault's inactivity is also apparent on ERT Profile 1 (Figure 5A). Note how the resistive top layer covers the fault, suggesting that the fault has not been active in recent times.

It was suggested by Kinabo et al. (2008) that some fault scarps are experiencing retreat as a result of erosion during the hiatus between episodes of faulting. In Lake Ngami, there was a single outcrop of fault breccia 2 km west of the Kunyere Fault scarp within the lake. The fault breccia is located near station 22 on MT Profile 1 (Figure 6C). Note how the resistive rocks extend well beyond the fault scarp and end near the breccia site. If the breccia site represents the original location of the Kunyere Fault, then it is apparent that erosion has caused the scarp to retreat which is a clear sign of tectonic inactivity. Also, note how the resistive anomaly near the breccia site on MT Profile 1 (Figure 6C) is not apparent on ERT Profile 1 (Figure 5A). The ERT profile depicts the area around the breccia site as conductive. We attribute the discrepancy between the two

data sets to differences in depth of penetration. MT data does not show the top 10 – 30 m of the subsurface; therefore, the penetration depths for MT data are deeper than ERT data. This suggests that the resistive breccia site cannot be seen in the graben on the ERT section because it is masked by the very conductive lake sediments that compose the top 30 m (e.g., Laletsang et al., 2008) of Lake Ngami. However, the MT profile is able to image the breccia site within the graben because the penetration depths is greater.

5.1.3 Thamalakane Fault

The MT Profile 2 model (Figure 7B) depicts the Thamalakane Fault as a broad conductive anomaly near the end of the profile with multiple vertical conductive zones throughout the remainder of the profile. Again, we interpret the conductive anomalies associated with the Thamalakane Fault as resulting from the presence of fluids which further suggests tectonic activity. Note how the calcretes on ERT Profile 2 are not covering the fault (Figure 5B). This observation is further confirmation that the Thamalakane Fault remains active.

The multiple areas of conductivity near the Thamalakane Fault arise from the fault being segmented along strike. Aeromagnetic maps (Figure 3C) as well as our ground survey (Figure 7A) clearly show that the fault contains multiple segments within the basement. Kinabo et al. (2008) describes the Thamalakane Fault as over lapping right stepping en-echelon fault segments that are visible on the surface as well. These segments are attributed to the characteristic fault-plane propagation associated with the other faults within the ORZ.

5.1.4 Mababe Fault

Careful observation of the Mababe graben on the DEM map (Figure 2A) shows two scarps associated with the Mababe depression that are about 7 km apart. A question concerning the inner most scarp is whether or not the scarp is a hydrographic/erosional scarp related to the shorelines of paleo-lake Mababe or if the inner scarp is geologically controlled. ERT Profile 4 (Figure 3D) and ground magnetic data (Figure 8C) suggest that the scarp is tectonically controlled. On ERT Profile 4, note how the Mababe Fault does not have substantial calcretes covering the fault which suggests active tectonic activity. A ~12 m drop in surface elevation and a >200 nT magnetic anomaly associated with this feature is further indication that the inner scarp is controlled by tectonics.

5.2 Source of Conductivity

The ERT and MT profiles for our study were acquired within the distal end of the Okavango Delta near the southern extent of the rift zone. Both the ERT and the MT results depict the ORZ subsurface within the grabens as a very conductive environment. The tectonically active faults associated with the ORZ show a characteristic FZC signature characteristic of active fault segments (e.g., SAF). The location of the faults based on the aeromagnetic maps with respect to the location of the delta (Figure 2) shows that the faults link up and extend into the delta, suggesting that a probable source for the highly conductive nature of the faults may be attributed to surface water and groundwater from the delta being channeled by the faults. Campbell et al. (2006) noted that fresh water within the Okavango Delta has a value of 9 – 30 Ohm.m while brackish water ranges from 3 – 8 Ohm.m and saline fluids are < 3 Ohm.m. MT Profile 2 (Figure 7B)

depicts the Thamalakane Fault near Maun as a large conductive anomaly with a resistivity value of < 5 Ohm.m, suggesting that this fault zone is channeling brackish to saline water directly from the Thamalakane River. Near Maun, tributaries from the Okavango Delta truncate against the Thamalakane Fault, causing the Thamalakane River to flow along the fault zone. Although we do not have MT data for the Kunyere Fault near Maun, several of the rivers extending from the delta also truncate against the fault. Similar to the Thamalakane Fault, this would allow water from the rivers to be channeled by the Kunyere Fault zone. We are also uncertain about whether or not the Mababe Fault is channeling fluids since we lack quality MT data for this area of the rift. Similar to Lake Ngami, the Mababe depression is a paleo-lake. Water was formerly supplied to the lake by the Kwando River prior to the river being diverted by uplift along the Linyanti Fault. Our ERT profile for the Mababe depression (Figure 5D) shows that the graben hosts very conductive sediments reaching resistivities as low as < 1 Ohm.m. The high conductivity values may be attributed to a thin film of saline fluid from evapotranspiration processes (e.g., McCarthy et al., 1991) coating the surface of the mineral grains. Milzow et al. (2009) explain that surface calcretes and silcretes, also known as duricrusts, form due to cementation of sand by silica and carbonate rich pore waters. Subsurface duricrusts form in the vadose zone close to the water table. Water table fluctuations lead to alternating saturated and unsaturated conditions which ultimately lead to duricrust precipitation. Calcretes form during saturated conditions while silcretes form during unsaturated conditions (Shaw and Nash, 1998). During the evapotranspiration process, transpiration by trees and evaporation processes cause the water table to fluctuate which enriches the subsurface with silica and carbonate salt

deposition. Within the Mababe depression, the source of the high conductivity may be due to sand grains that contain dissolved solutes (saline fluids) within the pore spaces of the sediments.

According to MT Profile 1 (Figure 6B), both the Tsau Fault and the Lecha Fault near Lake Ngami have conductive anomalies ranging from 5 - 10 Ohm.m that have propagated into the sedimentary cover. Our MT profile crosses the southwestern segments of the Tsau and Lecha faults which are located within the drier regions outside of the delta; however, note that both the Tsau and the Lecha Fault extend into the delta along strike in the northeast (Figure 2). This suggests that the conductivity for these faults is sourced from water being channeled by the faults in the northeast or by groundwater flow toward the dry regions outside the permanent and seasonal delta near Lake Ngami.

The lack of tectonic activity along the Kunyere Fault near Lake Ngami may suggest that the fault has been sealed by calcite/silica cement in this area, similar to the Sand Hill Fault in the Albuquerque basin, New Mexico. A study of the elongate patterns of cementation along the Sand Hill Fault led Mozley and Goodwin (1995) to conclude that calcite cements precipitated from subvertical flowing groundwater and are elongate parallel to the flow direction at the time of precipitation. Analogous to the faults of the ORZ, the Sand Hill Fault is located in an arid environment, where carbonate precipitation is the dominant process in weathering horizons (Mozely and Goodwin, 1995). Milzow et al. (2009) mention that the calcretes and silcretes that are mainly found in the distal parts of the Okavango Delta are attributed to the enrichment of silica and carbonates in the surface water down the flow gradient due to evapotranspiration processes (McCarthy and

Ellery 1995; Shaw and Nash, 1998). Our ERT and MT data show that the Kunyere Fault near Lake Ngami (Figure 5A and 6C) has not moved in recent times which may have allowed for past surface water and groundwater from the delta to flow vertically along the fault and accumulate precipitated calcite and silica cements which eventually sealed the fault. Fault movement and active deformation is generally (but not necessarily) required to maintain the interconnectivity of pore space within a rock. The lack of tectonic activity can cause solutes that are carried in the fluids being channeled by the faults to precipitate in the pore space and eventually seal the fluid pathways (Park and Wernicke, 2003; Hoffmann-Rothe et al., 2004).

It is possible that the Kunyere Fault near Lake Ngami does posses a FZC that is too narrow to be resolved by MT, similar to the Dead Sea Transform Fault (DST - the Arava Fault) located in the Arava valley in Jordan. The Arava Fault is an active left-lateral transform fault which lacks a distinct FZC. Ritter et al. (2003; 2005) attribute the absence of the FZC to a narrow damage zone (i.e., a broad highly permeable zone with an increase concentration of fractures, faults, and veins surrounding the fault core – Chester and Logan (1986); Caine et al. (1996); Evans et al. (1997); Ritter et al. (2005). The narrow damage zone implies that strain has been extremely localized upon a single, very narrow shear zone over long periods of time (Mitra and Ismat, 2001; Ritter et al., 2003; 2005). According to Ritter et al. (2005), the lack of a FZC in the brittle crust is coupled with the fault acting as a barrier to cross-fault fluid flow transport due to an impermeable fault seal, a lithological contrast across the fault, or some combination of the two.

In contrast to the active Arava Fault, we interpret the Kunyere Fault near Lake Ngami to be recently inactive; however, analogous to the Arava Fault, a FZC may exist

for the Kunyere Fault, but a narrow damage zone may cause the FZC to be too narrow to be imaged by the MT survey. The source (if any) of the conductivity within the damage zone could be attributed to water being channeled by the fault in the northeast near the delta or by groundwater flow outside the permanent and seasonal delta near Lake Ngami. If the Kunyere Fault has undergone cementation, it would cause the fault to act as an impermeable barrier to cross-fault groundwater flow, similar to the Arava Fault.

5.3 Fault Zone Architecture:

The Department of Water Affairs (e.g., DWA, 2004; Milzow et al., 2009) conducted a major groundwater exploration program from 1995 – 1997 and 2000 – 2004 to supply water to Maun and surrounding areas. Over 150 boreholes were drilled an average of 60 m below ground level in the distal regions of the delta near the Kunyere and Thamalakane faults. The boreholes revealed that the lithology both parallel and perpendicular to the faults consisted of clay, clayey, and silty sands inter-layered with fine-to-medium-grained sands. Fluctuations between wet and dry climatic periods are responsible for the large-scale inter-layering of these sediments. Wet periods allowed for clay-rich and silty sediments to be deposited along the faults from standing water from the delta being pooled directly against the faults while larger sand grains were deposited during drier periods when the delta was dominated by fluvial conditions. Near the Thamalakane and Kunyere faults, the sand-dominated lithology pinches out while the more clay-dominated layers thicken. The prevalence of clay material on or near the fault zones suggests that the faults act as effect barriers to lateral groundwater flow (DWA, 2004; Milzow et al., 2009). These observations may also suggest that the conductive

anomalies associated with the faults shown by our MT data are a result of clay content both parallel and perpendicular to the faults rather than brackish groundwater being channeled by the faults. Clay minerals can have very low resistivity values ranging from 5 – 20 Ohm.m (Palacky, 1987).

Our ERT and MT results combined with the observations made by the DWA and Milzow et al. (2009) may suggest that the fault zones are acting as both conduits and barriers to fluid flow. According to several authors (e.g., Chester and Logan, 1986; Caine et al., 1996; Evans et al., 1997; Ritter et al., 2005) the primary components that control fluid flow within a fault zone are fault core, damage zone, and protolith. The fault core is a narrow (centimeters – meters), often impermeable zone of highly deformed rock where the majority of slip is accommodated. The damage zone is a broad (up to hundreds of meters) highly permeable zone with an increased concentration of fractures and faults, while the protolith is the undeformed country rock. The fault core is dominated by grain size and/or mineral precipitation whereas in the damage zone, permeability is dominated by the hydraulic properties of fracture networks such as small faults, veins, fracture, cleavage, and folds. Whether a fault zone will act as a conduit, barrier, or combined conduit-barrier system is controlled by the relative percentage of fault core and damage zone structures and the variability in grain size and fracture permeability (Caine et al., 1996). For example, the clay-rich sediments surrounding the Kunyere and Thamalakane faults near Maun suggest that the fault cores in this area, where the delta comes in direct contact with the faults, would act as barriers to lateral groundwater flow perpendicular to the fault zones. Along strike towards the southwest near Lake Ngami, the calcite and/or silica-cemented fault breccia associated with the

Kunyere Fault suggests that the fault core in this area of the rift, where it is relatively dry, would act as post-deformational barriers to lateral fluid flow. However, the subsidiary fractures and splays in the damage zones of the ORZ faults suggest that the faults would also act as conduits for fluid flow within the fault zones. Multiple fault segmentation of individual faults along strike displayed on the aeromagnetic and SRTM maps combined with the localized fault splays and fractures depicted on our ERT and MT profiles reflect a combination of localized and distributed strain within the rift system. Combined strain localization and distributed deformation suggests a barrier-conduit permeability structure (Caine et al., 1996). The impermeable fault cores act as barriers to lateral groundwater flow between faults while the fractures, linements, and splays within the damage zones act as vertical conduits for fluid flow.

5.4 Differences in Magnetic Signatures

One characteristic of the faults associated with the ORZ that needs further attention is the differences in magnetic signatures of the faults. For example, the Mababe Fault and Gumare Fault exhibit a magnetic high on regional aeromagnetic maps. In contrast, the Tsau, Lecha, Kunyere, and Thamalakane faults all display a magnetic low (Figure 9). Several factors may be responsible for the differences in magnetic expression. One factor may be the influence of the Okavango Delta. As previously stated, the faults link up and extend into the delta in the northeast (Figure 2) which suggests that the conductivity displayed by several of the faults is sourced from surface

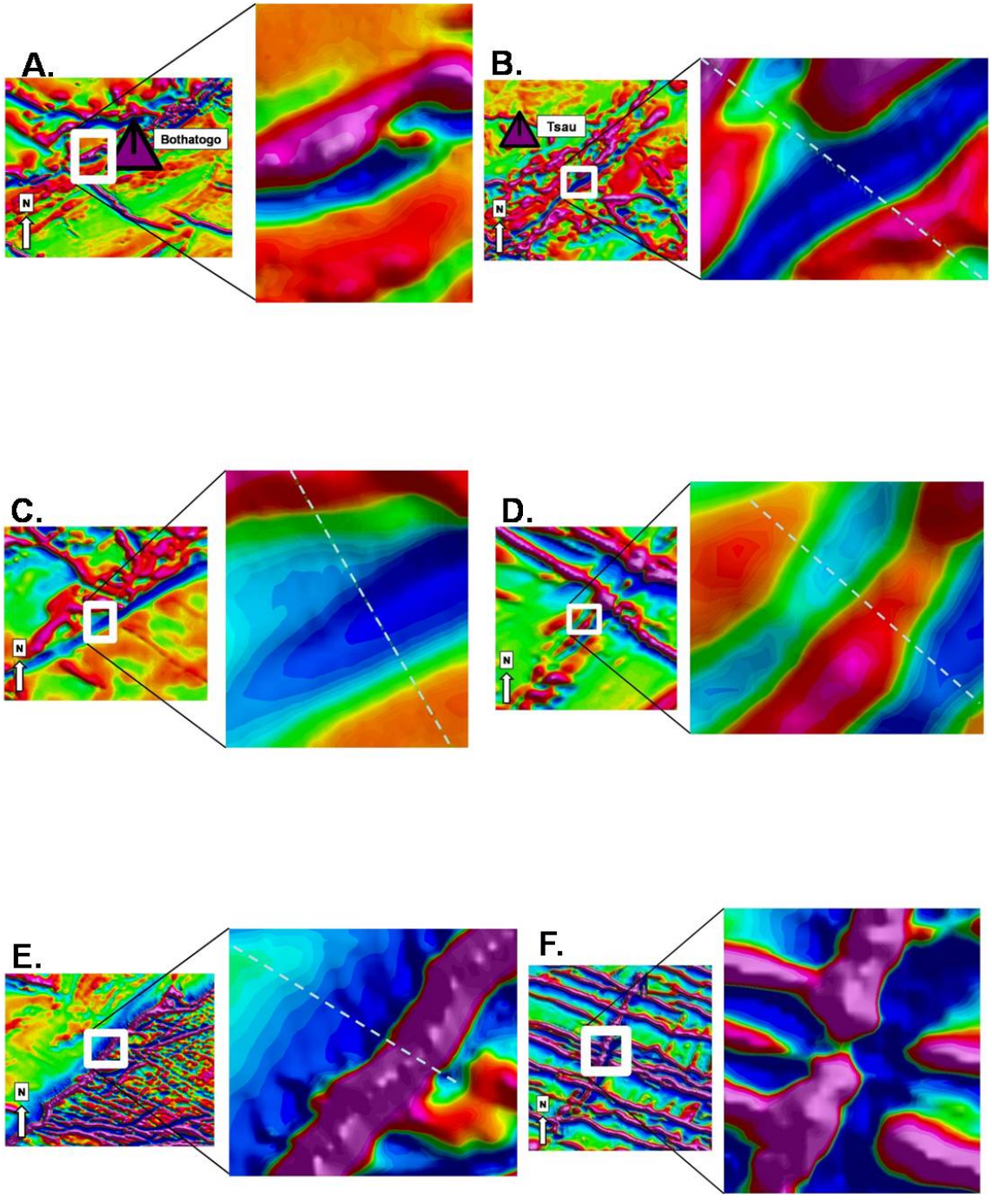

Figure 9. Enlarged vertical derivative aeromagnetic images of segments of the faults associated with the ORZ. A.) Southern Kunyere Fault. B.) Southern Tsau Fault. C.) Southern Lecha Fault. D.) Southern Thamalakane Fault. E). Mababe Fault. F.) Gumare Fault. Blue dashed lines delineate our magnetic acquisition profiles.

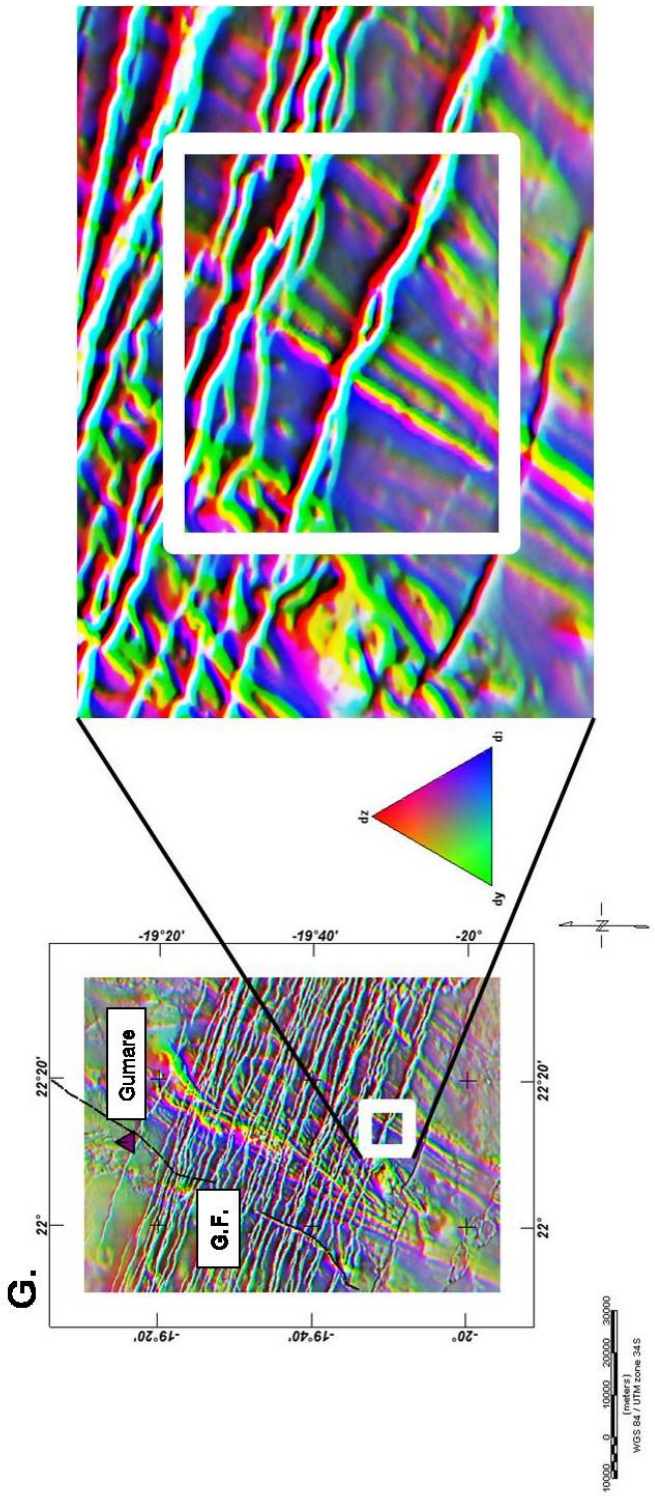

Figure 9 (cont). Ternary map showing the location of the conductive and magnetic anomaly along MT Profile 1 (stations 059 – 063) and magnetic Profile 1.

water and/or groundwater being channeled from the delta by the faults. A hypothesis proposed by Peirce et al. (1998) suggested that magnetization along faults may be caused by the commingling of fluids and rocks of contrasting redox potentials. The process involves iron being transported in oxidized waters flowing along vertical faults and fractures near basement rocks and the precipitation of exotic iron-bearing minerals during the ascent of the water as it undergoes redox reactions. The redox state of the rocks are based on mineralogy: highly oxidizing conditions prevail during deposition of evaporites (abundant hematite and anhydrite) while reducing environments occur during deposition of anoxic marine shales (pyrite and anhydrite)(Peirce et al., 1998). The Okavango Delta is a both a fluvial and lacustrine system where carbonate precipitation (i.e., evaporites) dominates. If the oxidized fluids being channeled by the fault zones flow deep enough to encounter basement rocks at high temperature conditions, redox reactions can liberate iron from the basement rocks. Geochemical reactions between iron and hematite, a mineral that occurs in hydrothermal and weathering environments, can result in the deposition of maghematite, a mineral with a high magnetic susceptibility. The deposition of maghematite would in turn cause a magnetic high on aeromagnetic maps (i.e., the Gumare Fault and the Mababe Fault). Weathering processes within fault zones due to fluid alteration where iron is not being precipitated could result in a magnetic low. Note that the majority of the faults that are expressed as magnetic lows (i.e., the Tsau, Lecha, Thamalakane, and Kunyere faults) are located at the distal end of the delta (Figure 2) and are interpreted to be conducting fluids, especially the Tsau, Lecha, and Thamalakane faults. This suggests that the magnetic lows for these faults are due to weathering processes from the presence of fluids within the fault zones. This observation also

suggests that redox reactions may be occurring in only certain parts of the delta. Reasons for the difference in location of magnetic and non-magnetic fault signatures include: 1.) current fluid flow status along the faults (i.e., no fluid flow means no redox reactions), 2.) chemistry of the groundwater during flow, and 3.) reactions that modify groundwater flow. The chemistry of the groundwater is likely to evolve during flow. In the case of the Okavango Delta, the groundwater becomes more saline down gradient from the beginning of the delta (McCarthy and Ellery, 1995; Shaw and Nash, 1998). Thus, faults that are close to the source of the delta encounter very different fluid chemistries than those that are more distal.

A second factor may be the extreme variability of the magnetic conditions within the rocks surrounding the faults. For example, parts of Thamalakane Fault occur between rocks of contrasting magnetic properties (i.e., the magnetic Kgwebe Formation and the non-magnetic Ghanzi Group rocks). Parts of the Kunyere Fault and Mababe Fault are lineaments that contrast shallow magnetic sources on the plateau (up-thrown) side of the faults to a down-thrown and deeply buried magnetic source in the basin side of the fault. These high contrast scenarios will be different when both sides of the fault have similar magnetic properties. The reason for the contrast in the magnetic signature of the faults is unknown; however, we attribute the contrast to fluid-rock interactions along the fault planes and/or differences in magnetic properties of the rocks on either side of the faults.

5.4.1. Fault Models

Grauch et al. (2001) performed a study over the Albuquerque basin within the Rio Grande Rift. They concluded from aeromagnetic surveys, profile and map analysis, and

studies of magnetic properties (i.e., magnetic susceptibilities) of core samples that faults within sedimentary basins can best be explained by juxtaposition of basin fill of differing magnetic properties. Their study provides insight on how the magnetic expression of faults in profile can range from symmetric curves with one inflection point to curves with two asymmetric peaks that have two or more inflection points. The symmetric curves can be modeled as a single magnetic layer juxtaposed against non-magnetic material. The asymmetric peaks are modeled by general geometry of a thin magnetic layer on the up-thrown side of the fault offset from a thicker magnetic layer on the down-thrown side of the fault, referred to as the "thin-thick" model. These models provide an alternative explanation for apparent fault-zone lows, compared to Mozley and Goodwin's (1995) conclusion that cementation along fault planes from past fluid flow can be responsible for loss of magnetization within a fault zone.

Our magnetic ground data profiles that we acquired over the Tsau, Lecha, Kunyere, Thamalakane, and Mababe faults have both symmetric and asymmetric appearances similar to the profiles discussed by Grauch et al. (2001). The reason for the contrast in the magnetic signature of the faults is unknown; however, we attribute the contrast to hydrological conditions along the fault planes and/or differences in magnetic properties on either side of the fault

MT Profile 1 depicts the Tsau Fault as a conductive anomaly which we interpret to be an active fault that has propagated into the shallow sediments. Our model (Figure 10A) displays the fault as a small magnetic low that has had very little influence on displacing basement material. Note how the basement rocks on Figure 9B are the same intensity on both sides of the fault. An interesting observation to note about the Tsau

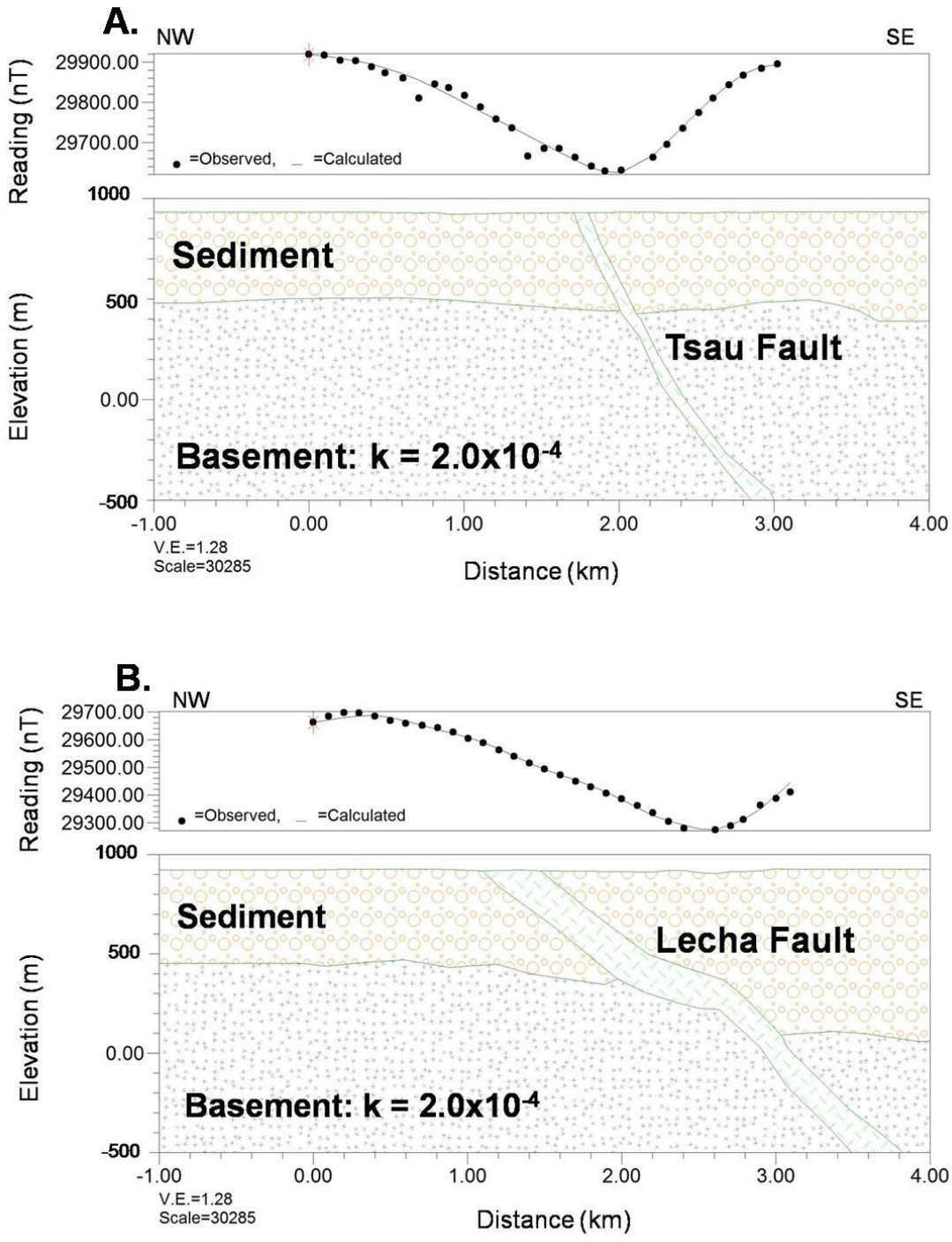

Figure 10. Magnetic models representing the A.) Tsau Fault and B.) Lecha Fault. Models were created using NGA's GM-SYS modeling program. Susceptibilities are in SI units.

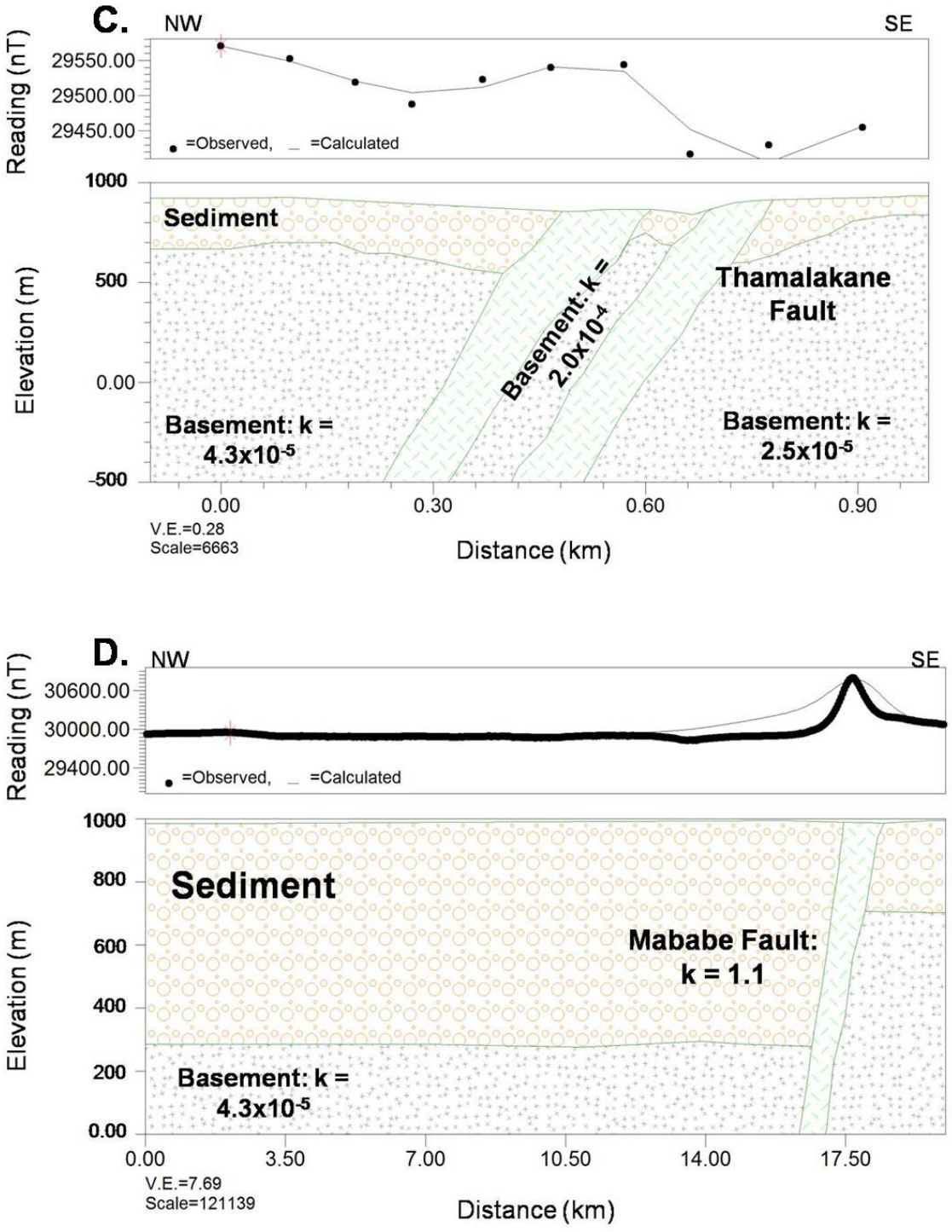

Figure 10 (cont). Magnetic models representing the C.) Thamalakane Fault and D.) Mababe Fault. Models were created using NGA's GM-SYS modeling program. Susceptibilities are in SI units.

Fault is that the fault cannot be seen on the aeromagnetic map until the first vertical derivative of the aeromagnetic data is taken.

The Lecha Fault, which we interpret to be a tectonically active fault that has propagated into the sedimentary cover, is shown as a large well-defined low-magnetic linear feature (Figure 10B). Aeromagnetic maps indicate that the Lecha Fault has displaced basement material (Figure 9C); therefore, the model honors this observation by displacing the basement rocks on the up-thrown and down-thrown blocks by a few 100 m.

The Thamalakane Fault (Figure 10C) is interpreted to be a tectonically active fault which exhibits some displacement within the basement. It is depicted as a linear magnetic low on the aeromagnetic map similar to the Kunyere, Tsau, and Lecha faults; however, the magnetic intensity of the basement and/or dikes on both sides of the fault remains fairly consistent throughout majority of the fault with small areas of displacement along strike towards the north (Figure 9D). The model separates the fault into two low-magnetic faults with an area of high magnetic material between the two faults. The up-thrown and down-thrown basement blocks both exhibit lower magnetic susceptibilities than the rock between the two faults.

The Mababe model (Figure 10D) represents the fault as a large magnetic high with significant vertical displacement of the basement material towards the northwest. The aeromagnetic maps depict the Mababe Fault as a very strong magnetic high followed by a sharp break into a magnetic low (Figure 9E). The same characteristic high is exhibited by the Gumare Fault (Figure 9F). The signature magnetic high displayed by the Mababe and Gumare faults are opposite that of the Tsau, Lecha, Kunyere, and

Thamalakane faults, which are all characterized by linear magnetic lows rather than magnetic highs. The composition of the fault is unknown; however, it is apparent that the fault zone consists of minerals with high magnetic susceptibilities. It has been suggested that the magnetic high associated with the Mababe Fault may be attributed to the accumulation of magnetic sands along shorelines of paleo-lake Mababe. Similar magnetic sands have been observed along the shores of Lake Mweru in Zambia.

5.4.2. Gravity Models

Our gravity models for the Lake Ngami depression (Profile 1) and the Mababe depression (Profile 4) were created from our gravity ground surveys. Our interpretation for the Ngami gravity profile (Figure 11A) depicts the Lake Ngami graben to be bounded by the Kunyere and Lecha faults. A second graben is also defined near the beginning of the model. We interpret the second graben to be possibly bounded by a fault to the northwest. The northwestern flank of the graben closely coincides with the location of the strong conductor depicted by MT Profile 1 (stations 059 – 063) (Figure 6 A3) and the magnetic anomaly present on the magnetic Profile 1 (Figure 6 A2). The presence of the potentially active fault may be an indication of how the rift is currently widening over time by reactivation of basement structures. The fault may have resulted from the reactivation of a limb of a basement fold that was tectonically active before the

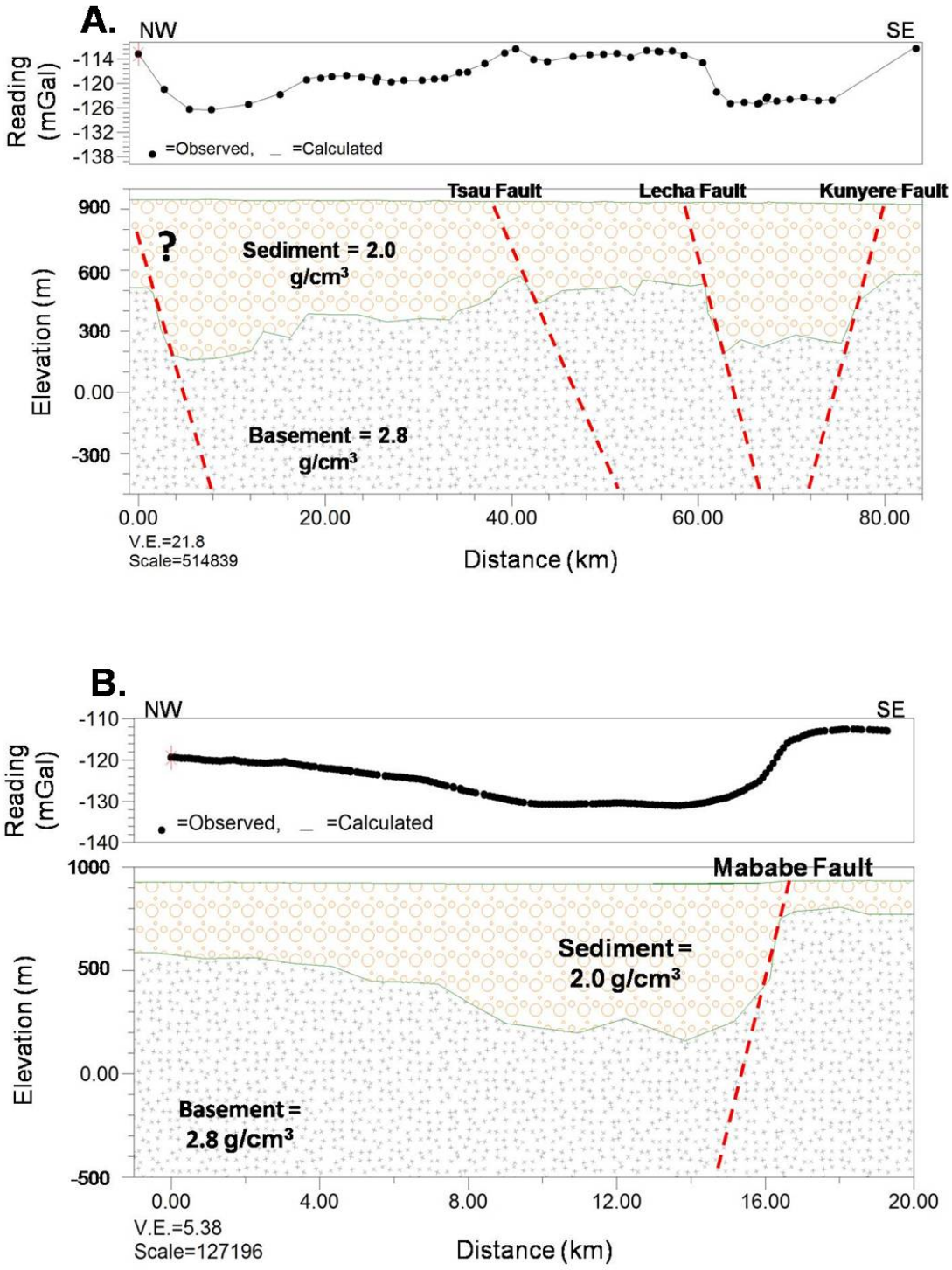

Figure 11. Gravity models representing A.) Profile 1 through the Ngami graben and B.) Profile 4 through the Mababe depression. Dashed lines delineate fault locations. Models were created using NGA's GM-SYS modeling program.

appearance of the Karoo dike swarm (Figure 9G). The regional gravity data of the area (Figure 4A) displays a large linear gravity high near the town of Gumare that directly corresponds with the position of the basement fold. Most linear gravity features are associated with rifting processes which suggests that the entire basement fold may have been a failed ancient rift.

The shape of the graben is in the form of synformal depressions suggesting that the basin is in an early stage of development. The Mababe model (Figure 11B) shows the shape of the Mababe depression to have the appearance of a more developed half-graben. Our models are consistent with the Kinabo et al. (2007) observation that the Mababe depression is in a more advanced stage of development than the Lake Ngami depression. Their study concludes that the Kunyere Fault is the main boundary fault near Lake Ngami (Modisi, 2000). Towards the north, displacement along the Kunyere Fault wanes and strain is accommodated by the Mababe Fault via the Thamalakane Fault, making the Mababe Fault the main boundary fault within the Mababe graben.

5.5 Seismicity

A study of the San Andreas Fault (SAF) conducted by several authors (e.g., Unsworth et al., 1997; Mackie et al., 1998; Unsworth et al., 1999, Unsworth et al., 2000; Bedrosian et al., 2004; Unsworth and Bedrosian, 2004; Ritter et al., 2005) suggest that seismic behavior may be controlled by a connected network of fluid-filled cracks within fault zones. Along the SAF, there is marked seismic variability, with some segments characterized by infrequent, large-magnitude earthquakes while others exhibit abundant microseismicity and aseismic creep (Allen, 1968). The SAF is characterized by a

creeping central segment near Hollister, CA. At Parkfield, CA, the fault is in a transition zone between a creeping segment to the north and a locked segment to the south. The SAF near Carrizo Plain, CA has been locked since 1875 (Ritter et al., 2005). The Hollister creeping segment is characterized by a 750-m wide damage zone (i.e., a region of pervasive fracturing (Caine et al., 1996)) and localized zones of high conductivity at depth separated from one another by northeast dipping impermeable fault seals in the upper 2 – 3 km (8 km at most) between the SAF and the Calaveras Fault (Bedrosian et al., 2004; Ritter et al., 2005). Similar to Hollister, the SAF at Parkfield consists of a broad damage zone (~ 750 m) and an anomalously high conductive zone centered on the fault extending from the surface to a depth of 2 – 5 km (Ritter et al., 2005). These zones of high conductivity, FZC's, source their high conductivity values from saline fluid-filled voids and factures within the brecciated and damaged zone of the fault (Anderson et al., 1983; Caine et al., 1996). In contrast, a narrow FZC is associated along the locked segment of the SAF near Carrizo Plain (Unsworth et al., 1999). Here, the rock is resistive, crystalline, and devoid of fluid pathways (Bedrosian et al., 2004).

The locations of the FZCs at Hollister and Parkfield coincide with zones of reduced seismic velocity and enhanced V_p/V_s (where V_p/V_s is the ratio of compressional wave velocity to shear-wave velocity)(Thurber et al., 1997, 2003; Catchings et al., 2002). Both Hollister and Parkfield experience abundant microseismicity, especially at Hollister where there is a distinct absence of earthquakes with magnitudes greater than 5. The Carrizo Plain, in contrast, suffers large, damaging earthquakes such as the 1857 Forth Tejon quake (M = 7.8; Ellsworth, 1990; Ritter et al., 2005). These observations reveal a correlation between FZC magnitude and seismicity. The creeping segment at Hollister

and the transition segment at Parkfield both contain wide FZCs and broad damage zones that allow ample fluids to occupy and migrate between pore spaces within the rocks (fault zone conductance). The seismicity associated with the SAF at both locations is characterized by abundant seismicity and a lack of severe earthquakes. In contrast, the locked segment near Carrizo Plain is characterized by a smaller FZC and a narrow zone of deformation with only small quantities of fluid present (Unsworth et al., 1999). Here, the earthquakes are infrequent and damaging. This suggests that the fluids associated with the strong FZCs near Hollister and Parkfield are enhancing microseismicity by increasing pore pressure through fluid migration along interconnecting faults and fractures (Townsend & Zoback, 2000; Unsworth et al., 2000; Ritter et al., 2005). Fluid migration causes high pore pressure within the rock. The high pressure, in turn, ultimately reduces shear stress from the rock (i.e., earthquakes are weak) so that stress does not build to higher levels over time, which generates larger magnitude earthquakes. The shallow and weak FZC near Carrizo Plain may be imaging a closing fracture network across the entire fault zone (i.e., cementation and sealing processes are in operation)(Ritter et al., 2005).

Seismicity and fluid flow may have a direct relationship with faulting in the ORZ, similar to the SAF. The Kunyere Fault may be exhibiting similar locked and creeping segments as the SAF in California. Near Lake Ngami, the fault lacks a significant FZC and shows evidence of fault scarp retreat due to recent inactivity. Along strike to the northeast near Maun, seismicity increases substantially between the Kunyere Fault and the Thamalakane Fault, where strain is being transferred from the Kunyere Fault to the Thamalakane Fault (Figure 12). Earthquakes in this area are predominantly weak, except

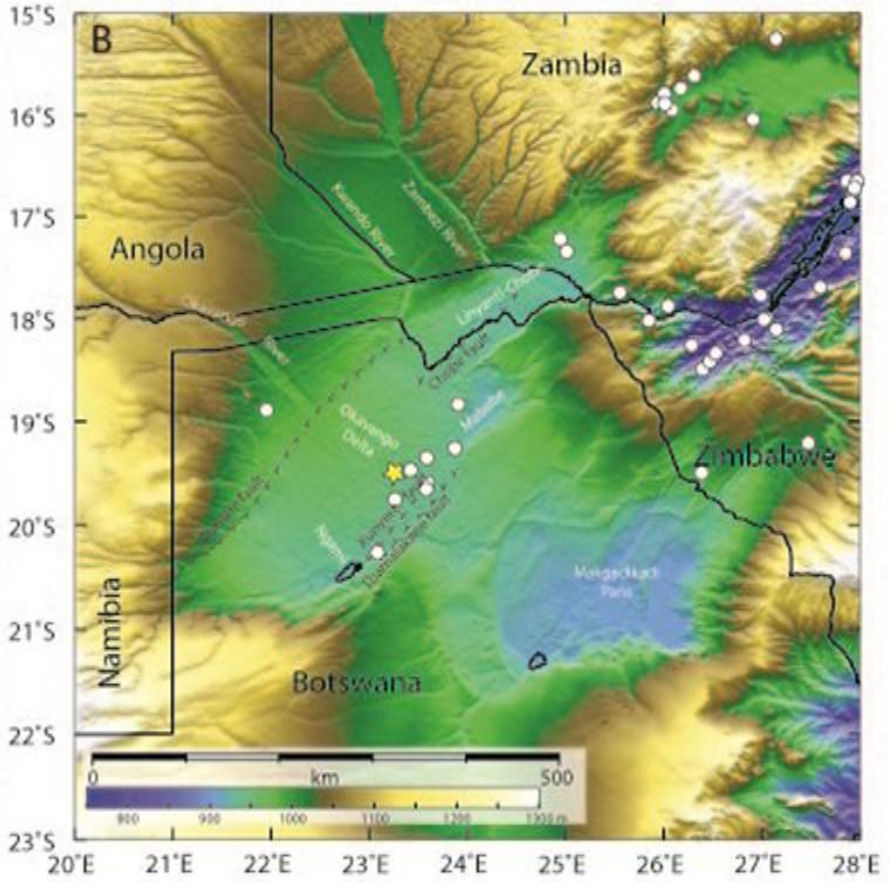

Figure 12. Seismicity map of the ORZ. White circles indicate areas of seismicity. The star indicates the location of the 1952 magnitude 6.7 earthquake (courtesy of Dr. Canales).

for the large earthquake events that were recorded during the May 1952 – May 1953 period, with magnitudes ranging between 5.0 and 6.7 on the Richter scale (Hutchins et al., 1976; Milzow et al., 2009). The Thamalakane Fault is interpreted to be channeling fluids in this area, suggesting that the northern segment of the Kunyere Fault may also be channeling fluids. These observations suggest that the southern segment of the Kunyere Fault near Lake Ngami may be locked with resultant calcite/silica cement precipitation, similar to the SAF near Carrizo Plain. The Arava Fault in Jordan, which also lacks a FZC similar to the Kunyere Fault, is nearly devoid of recent seismicity (Ambraseys and Jackson, 1998). However, seismic networks in this area have only been in operation since the 1980s and several magnitude 7 events can be confidently attributed to the Arava Fault within the last millennia (Klinger et al., 2000b). The microseismicity and lack of damaging earthquakes associated with the northern segments between the Kunyere Fault and the Thamalakane Fault suggest that fluids within the fault zones and splays may suggest that pore pressure is being raised in this area of the rift and reducing shear stress. MT Profile 2 (Figure 7B) shows the Thamalakane Fault as a wide conductive anomaly (~ 4 km) with multiple vertical conductive zones that reach as deep as ~ 300 m throughout the remainder of the profile. The conductive anomalies associated with the Tsau Fault and the Lecha Fault near the Lake Ngami area are smaller, weaker, and much shallower (~100 m) especially the Tsau Fault anomaly (Figure 6B). This observation further enhances the observation made by Kinabo et al. (2008) that tectonic activity near Lake Ngami is wanning as the fracture network closes due to sealing and cementation.

A study performed by Brodsky and Kanamori (2001) suggests that lubrication by a viscous fluid within a fault zone can reduce the frictional stress during large

earthquakes (M>4) by as much as 30%. The study suggested that any large earthquake that produces a slip distance of greater than a few meters along a fault plane during a single earthquake event will have a zone of the fault that is well lubricated. Lubrication also reduces high frequency energy due to contacting asperities during an earthquake. Consequently, large slip displacement and reduction in high frequency energy result in less damage. The fluids being channeled by the faults in the ORZ may allow for easier slip along the fault planes during large earthquakes. Additional geophysical and hydrologic data are required to further understand the relationship between crustal fluids and seismic behavior.

CHAPTER VI

CONCLUSION

The conclusions of our study of fault characteristics within the ORZ are as follows:

1. MT data depict conductive anomalies associated with the Tsau, Lecha, and Thamalakane faults, but no conductive anomaly associated with the Kunyere Fault. The lack of a conductive anomaly associated with the Kunyere Fault and calcretes covering the fault on ERT data suggest possible inactivity, a sealed fault, or represents an erosional scarp. The Tsau Fault and the Lecha Fault cut through the sedimentary cover and are interpreted to be channeling fluids, suggesting either post sedimentation activity or reactivation in recent times.
2. The faults associated with the ORZ extend into the delta suggesting that surface water and/or brackish to saline groundwater from the Okavango Delta is the source of the conductive anomalies.
3. The relationship between the impermeable lithologies surrounding the fault cores and the abundance of minor faults, fractures, and splays within the damage zones of the fault zones suggest that the faults are acting as both conduits and barriers to fluid flow.

4. The differences in magnetic character of the faults within the basement may be related to the precipitation of iron-bearing minerals through redox reactions or weathering processes as fluids are being channeled along the faults. The differences may also be caused by varying magnetic properties on either side of the fault.
5. The lack of strong violent earthquakes within the ORZ may be attributed to fluids occupying and migrating between pore spaces within the fault zone which causes increased pore pressure, thereby reducing the shear stress required for rupture. The reduction in shear stress allows for microseismicity and a lack of severe earthquakes. Fluids being conducted by the faults may also enhance slip along fault planes, causing the rift to lengthen and widen more rapidly over time.

CHAPTER VII

FUTURE WORK

Research within the ORZ has provided excellent insight into the embryonic stages of continental rifting; however, many unanswered questions remain. Basement fabric appears to have a significant influence on fault orientation; however, other factors such as mantle processes and extensional stress components directly beneath the ORZ should be investigated to assess fault placement and basin subsidence within the rift. Thus far, critical information concerning the Kunyere, Thamalakane, Tsau, Lecha, and Mababe fault systems has been acquired; however, little is known about the youngest faults (i.e., the Gumare, Phuti, and Nare faults) and the role they play in the evolution of the rift. Since the faults are still considered to be very young, geophysical surveys across these faults would continue to increase our knowledge of nascent rifting processes. Continued seismic investigations (reflection and refraction studies) and geophysical surveys that penetrate deep within the subsurface should also be utilized to present a clearer image of what is occurring at depth in terms of fault linkage and propagation. Deeper geophysical investigations can also examine exactly how deep the conductive anomalies near the fault zones extend within the subsurface to shed some light on the role of fluids in fault development, propagation, magnetic properties, and possibly seismicity. These results may provide identification of how much water is lost from the Okavango Delta through

the faults. Our interpretation that the faults associated with the ORZ are serving as conduits for fluids may imply that some of the annual discharge from the delta may be lost by fluid flow within the fault zones and not entirely attributed to evapotranspiration. A study performed by Ramberg et al. (2006a) revealed that direct evaporation from surface water was calculated to amount to 9 – 12% of the annual inflows, leaving approximately 90% of the inflow to be infiltrated into the groundwater system and removed by evaporation and transpiration from plants. McCarthy (2006) noted that due to faulting, the basement rocks beneath the delta are highly fractured and groundwater could possibly leave the area along these discrete pathways. In terms of the Okavango Delta water budget, the results of our study suggest that inflows infiltrating the delta are leaving the system by both evapotranspiration processes and fluid migration along fault zones.

REFERENCES

Akanyang, P., 1997, The geology of the Lake Ngami area: Geological Survey Botswana, Bulletin 42, p. 33p.

Allen, C., 1986, The tectonic environments of seismically active and inactive areas along the San Andreas fault system. In: Dickinson, W. and Grantz, A. (eds) Proceedings of Conference on Geologic Problems of the San Andreas Fault System, p. 70 - 82.

Ambraseys, N.N.a.J., J.A., 1998, Faulting associated with historical and recent earthquakes in the Eastern Meaditerranean region: Geophysical Journal International, v. 133, p. 390 - 406.

Anderson, J.L., Osbourne, R.H., and Palmer, D.F., 1983, Cataclastic rocks of the San Gabriel fault: an expression of deformation at deeper levels in the San Andreas fault zone: Tectonophysics, v. 98, p. 209 - 251.

Aubourg, C., Tshoso, G., Le Gall, B., Bertrand, H., Tiercelin, J.-J., Kampunzu, A.B., Dyment, J., and Modisi, M.P., 2008, Magma flow revealed by magnetic fabric in the Okavango giant dyke swarm, Karoo igneous province, northern Botswana: Journal of Volcanology and Geothermal Research, v. 170, p. 247 - 261.

Ballard, S., Pollack, H.N., and Skinner, N.J., 1987, Terrestrial heat flow in Botswana and Namibia: Journal of Geophysical Research, v. 92, p. 6291 - 6300.

Bedrosian, P.A., Unsworth, M.J., Egbert, G.D., and Thurber, C.H., 2004, Geophysical images of the creeping segment of the San Andreas fault: implications for the role of crustal fluids in the earthquake process: Tectonophysics, v. 385, p. 137 - 158.

Brodsky, E.E., and Kanamori, H., 2001, Elastohydrodynamic lubrication of faults: Journal of Geophysical Research, v. 106, p. 16,357 - 16,374.

Byerlee, J., 1993, Model for episodic flow of high-pressure water in fault zones before earthquakes: Geology, v. 21, p. 303 - 306.

Caine, J.S., Evans, J.P., and Foster, C.B., 1996, Fault zone architecture and permeability structure: Geology, v.24, p. 1025 – 1028.

Campbell, G., Johnson, S., Bakaya, T., Kumer, H., Nsatsi, J., 2006, Airborne geophysical mapping of aquifer water quality and structural controls in the Lower Okavango Delta, Botswana: South African Journal of Geology, v. 109, p. 475 - 494.

Caputo, R., Piscitelli, S., Oliveto, A., Rizzo, E., and Lapenna, V., 2003, The use of electrical resistivity tomographies in active tectonics: Examples from the Tyrnavos Basin, Greece: Journal of Geodynamics, v. 36, p. 19 - 35.

Catchings, R., Rymer, M., Goldman, M., Hole, J., Huggins, R., and Lippus, C., 2002, High-resolution seismic velocities and shallow structure of the San Andreas fault zone at Middle Mountain, Parkfield, California: Bulletin of the Seismological Society of America, v. 92, p. 2493 - 2503.

Chapman, D.S., and Pollack, H.N., 1977, Heat flow and heat production in Zambia: Evidence for lithospheric thinning in central Africa: Tectonophysics, v. 41, p. 79 - 100.

Chester, F.M., and Logan, J.M., 1986a, Composite planar fabric of gouge from the Punchbowl fault, California: Journal of Structural Geology, v. 9, p. 621 - 634.

Chester, F.M., and Logan, J.M., 1986b, Implications for mechanical properties of brittle faults from observations of the Punchbowl fault zone, California: Pure and Applied Geophysics, v. 124, p. 79 - 106.

Chorowicz, J., 2005, The East African rift system: Journal of African Earth Sciences, v. 43, p. 379 - 410.

Cooke, H.J., 1984, The evidence from northern Botswana of climate change. In: Vogel, J. (Eds.), Late Cenozic palaeoclimates of the southern hemisphere. Balkema, Rotterdam, pp. 265 - 278

D.W.A., 2004, Maun Groundwater Development Project: phase 2, resources assement and field development. TB 10/3/2000 - 2001. Final report volume 1, main report: Ministry of Minerals Energy and Water Resources, Gaborone, Botswana.

Diaferia, I., Barchi, M., Loddo, M., Schiavone, D., and Siniscalchi, A., 2006, Detailed imaging of tectonic structures by multiscale earth resistivity tomographies: The Colfiorito normal faults (central Italy): Geophysical Research Letters, v. 33.

Dincer, T., Hutton, L.G., Kupree, B.B.J., 1978, Study, using stable isotopes, of flow distribution, surface-groundwater relations and evapotranspiration in the Okavango Swamp, Botswana. STI/PUB/493, IAEA Symposium on Isotope Hydrology, IAEA, Neuherberg, Germany, p. 3 - 26.

Ebinger, C.J., 1989, Tectonic development of the western branch of the East African Rift System: Geological Society of America, Bulletin 101, p. 885 - 903.

Ebinger, C.J., 2005, Continental rifting and breakup processes: Insights from East Africa. In: Extended abstracts on the International Conference of the East African Rift System - EAR05: Geodynamics, Environment, Resources, and Sustainable Development, Mbeya, Tanzania, Edited by Atekwana et al., University of Dar es Salaam, Geology and Geography Departments.

Ebinger, C.J., Yemane, T., WoldeGabriel, G., Aronson, J., and Walter, R., 1993, Eocene - recent volcanism and faulting in the southern Main Ethiopian Rift: Journal of the Geological Society, London, v. 150, p. 99 - 108.

Ellsworth, W.L., 1990, Earthquake history, 1769 - 1989. In: Wallace, R. (ed.) The San Andreas Fault System, California: US Geological Survey, Professional Paper, v. 1515, p. 153 - 188.

Evans, J.P., Forster, C.B., and Goddard, J.V., 1997, Permeability of fault-related rocks and implications for hydraulic structure of fault zones: Journal of Structural Geology, v. 19, p. 1393 - 1404.

Fairhead, J.D., and Girdler, R.W., 1969, How far does the rift system extend through Africa?: Nature, v. 221, p. 1018 - 1020.

Furman, T., 2007, Geochemistry of East African Rift basalts: An overview: Journal of African Earth Sciences, v. 48, p. 147 - 160.

Gamrod, J.L., 2009, Paleolimnological Records of Environmental Change Preserved in Paleo-Lake Mababe, Northwest Botswana: Thesis (unpul), Oklahoma State University, p. 1 - 43.

Garstang, M., Ellery, W.N., McCarthy, T.S., Scholes, M.C., Scholes, R.J., Swap, R.J., Tyson, P.D., 1998, The contribution of aersol- and water-borne nutrients to the functioning of the Okavango Delta ecosystem, Botswana: South African Journal of Science, v. 94, p. 223 - 229.

George, R., Rogers, N., and Kelley, S., 1998, Earliest magmatism in Ethiopia: evidence for two mantle plumes in one flood basalt province: Geology, v. 26, p. 923 - 926.

Girdler, R.W., 1975, The great Bouguer anomaly over Africa: EOS (Transactions, American Geophysical Union), v. 56, p. 516 - 519.

Grauch, V.J.S., Hudson, M.R., and Minor, S.A., 2001, Aeromagnetic expression of faults that offset basin fill, Albuquerque basin, New Mexico: Geophysics, v. 66, p. 707 - 720.

Grove, A.T., 1969, Landforms and Climatic Change in Kalahari and Ngamiland: Geographical Journal, v. 135, p. 191 - 212.

Gumbricht, T., and McCarthy, T.S., 2003, Spatial Patterns of Island and Salt Crusts in the Okavango Delta, Botswana: South African Geographical Journal, v. 85, p. 164 - 169.

Hendrie, D.B., Kusznir, N.J., Morley, C.K., and Ebinger, C.J., 1994, Cenozoic extension in northern Kenya: a quantitative model of rift basin development in the Turkana region: Tectonophysics, v. 236, p. 409 - 438.

Hoffmann-Rothe, A., Ritter, O., and Janssen, C., 2004, Correlation of electrical conductivity and structural damage at a major strike-slip fault in north Chile: Journal of Geophysical Research, v. 109.

Hutchins, D.G., Hutton, S.M., Jones, C.R., and Loernhert, E.P., 1976, A summary of the geology, seismicity, geomorpholoygy and hydrogeology of the Okavango Delta: Department of Geologic Surveys, Gaborone, Botswana.

Jones, A.G., 1992, Electrical conductivity of the continental lower crust: In: Continental Lower Crust, p. 81 - 143.

Kampunzu, A.B., Bonhomme, M.G., and Kanika, M., 1998, Geochronology of volcanic rocks and evolution of the Cenozoic Western branch of the East African rift system: Journal of African Earth Sciences, v. 26, p. 441 - 461.

Kinabo, B.D., Atekwana, E.A., Hogan, J.P., Modisi, M.P., Wheaton, D.D., and Kampunzu, A.B., 2007, Early structural development of the Okavango rift zone, NW Botswana: Journal of African Earth Sciences, v. 48, p. 125 - 136.

Kinabo, B.D., Hogan, J.P., Atekwana, E.A., Abdelsalam, M.G., and Modisi, M.P., 2008, Fault growth and propagation during incipient continental rifting: Insights from a combined aeromagnetic and Shuttle Radar Topography Mission digital elevation model investigation of the Okavango Rift Zone, northwest Botswana: Tectonics, v. 27, p. 1 - 16.

Klinger, Y., Avouac, J.P., Karaki, N.A., Dorbath, L., and Tisnerat, N., 2000b, Seismic behavior of the Dead Sea fault along the Araba valley, Jordan: Geophysical Journal International, v. 142, p. 769 - 782.

Knight, K., Furman, T., and Bryce, J.G., 2003, 40 million years of mafic volcanism in Turkana, Kenya: geochemical insights: EOS (Transactions, American Geophysical Union 48), Fall Meeting Supplement, Abstract S52J - 04.

Laletsang, K., Modisi, M.P., Shemang, E.M., Moffat, L., and Moagi, O.R., 2007, Shallow seismic refraction and magnetic studies at Lake Ngami, The Okavango Delta, Northwest Botswana: Journal of African Earth Sciences.

Mackie, R.L., Livelybrooks, D.W., Madden, T.R., and Larsen, J.C., 1997, A magnetotelluric investigation of the San Andreas fault at Carrizo Plain, California: Geophysical Research Letters, v. 24, p. 1847 - 1850.

McCarthy, T.S., 2006, Groundwater in the wetlands of the Okavango Delta and its contribution to the sturcture and function of the ecosystem: Journal of Hydrology, v. 320, p. 264 - 282.

McCarthy, T.S., and Ellery, W.N., 1995, Sedimentation of the distal reaches of the Okavango Fan, Botswana and its bearing on calcrete and silcretes (ganister) formation: Journal of Sedimentary Research, v. A65, p. 77 - 90.

McCarthy, T.S., and Ellery, W.N., 1998, The Okavango Delta: Transactions of the Royal Society of South Africa, v. 53, p. 157 - 182.

McCarthy, T.S., McIver, J.R., and Verhagen, B.Th., 1991a, Groundwater evolution, chemical sedimentation and carbonate brine formation on an island in the Okavango Delta swamp, Botswana: Applied Geochemistry, v. 6, p. 577 - 595.

McCarthy, T.S., Smith, N.D., Ellery, W.N., and Gumbricht, T., 2001, The Okavango Delta - semiarid alluvial-fan sedimentation related to incipient rifting. In: Renaut, R.W., and Ashley, G.M. (eds), Sedimentation in Continential Rifts, SEPM (Society for Sedimentary Geology) Special Publications, v. 70, p. 179 - 193.

McCarthy, T.S., Stanistreet, I.G., and Cairncross, B., 1991b, The sedimentary dynamics of active fluvial channels on the Okavango (Delta) alluvial fan, Botswana: Sedimentology, v. 38, p. 471 - 487.

Milzow, C., Kgotlhang, L., Bauer-Gottwein, P., Meier, P., and Kinzelbach W., 2009, Regional review: the hydrology of the Okavango Delta, Botswana - processes, data and modelling: Hydrogeology Journal, v. 17, p. 1297 - 1328.

Mitra, G., and Ismat, Z., 2001, Microfracturing associated with reactivated fault zones and shear zones: what can it tell us about deformation history? In: Holdsworth, R.E., Strachan, R.A., Magloughlin, J.F., and Knipe, R.J. (eds) The Nature and Tectonic Significance of Fault Zone Weakening: Geological Society, London, Special Publications, v. 186, p. 113 - 140.

Modie, B.N., 2000, Geology and mineralisation in the Meso- to Neoproterozic Ghanzi-Chobe Belt of northwest Botswana: Journal of African Earth Sciences, v. 30, p. 467 - 474.

Modisi, M.P., 2000a, Fault systems at the southeastern boundary of the Okavango Rift, Botswana: Journal of African Earth Sciences, v. 30, p. 569 - 578.

Modisi, M.P., Atekwana, E.A., Kampunzu, A.B., and Ngwisanyi, T.H., 2000b, Rift kinematics during the incipient stages of continental extension: Evidence from the nascent Okavango rift basin, northwest Botswana: Geology, v. 28, p. 939 - 942.

Moore, A.E., and Larkin, P., 2001, Drainage evolution in south-central Africa since the breakup of Gondwana: South African Journal of Geology, v. 104, p. 47 - 68.

Morley, C.K., 2002, Evolution of large normal faults: Evidence from seismic reflection data: American Association of Petroleum Geologists, Bulletin 86, v. 6, p. 961 - 978.

Morley, C.K., Wescott, W.A., Stone, D.M., Harper, R.M., Wigger, S.T., and Karanja, F.M., 1992, Tectonic evolution of the northern Kenya Rift: Journal of the Geological Society, London, v. 149, p. 333 - 348.

Mozley, P.S., and Goodwin, L.B., 1995, Patterns of cementation along a Cenozoic normal fault: A record of paleoflow orientations: Geology, v. 23, p. 539 - 542.

Ochieng, J.O., Wilkinson, A.F., Kagasi, J., and Kimomo, S., 1988, Geology of the Loiyangalani area: Report 107 (Reconnaissance) Republic of Kenya Ministry of Environmental and Natural Resources, Mine and Geology Department, p. 55pp.

Palacky, G., 1987, Resistivity characteristics of geologic targets, in Naibighian, M.N., ed., Electromagnetic methods in applied geophysics: Tulsa Oklahoma, Society of Exploration Geophysicists, v. 1, p. 53.

Park, S.K., and Wernicke, B., 2003, Electrical conductivity images of Quaternary faults and Tertiary detachments in the California Basin and Range: Tectonics, v. 22, p. 4-1 - 4-9.

Peirce, J.W., Goussev, S.A., Charters, R.A., Abercrombie, H.J., and DePaoli, G.R., 1998b, Intra-sedimentary magnetizatin by vertical fluid flow and exotic geochemistry: The Leading Edge, v. 17, p. 89 - 92.

Pellant, C., 2002, Rocks and Minerals: London, Dorling Kindersley Limited, 254 p.

Ramberg, L., Wolski, P., Krah M., 2006a, Water balance and infiltration in a seaonal floodplain in the Okavango Delta, Botswana: Wetlands, v. 26, p. 677 - 690.

Reeves, C.V., 1972, Rifting in the Kalahari: Nature, v. 237, p. 95 - 96.

Ringrose, S., Huntsman-Mapila, P., Kampunzu, A.B., Downey, W., Coetzee, S., Vink, B., Matheson, W., and Vanderpost, C., 2005, Sedimentological and geochemical

evidence for palaeo-environmental change in the Makgadikgadi subbasin, in relation to the MOZ rift depression, Botswana: Palaeogeography Palaeoclimatology Palaeoecology, v. 217, p. 256 - 287.

Ritter, O., Hoffmann-Rothe, A., Bedrosian, P.A., Weckmann, U., and Haak, V., 2005, Electrical conductivity images of active and fossil fault zones. From: Bruhn, D. and Burlini, L. (eds) 2005. High-Strain Zones: Structure and Physical Properties: Geological Society of London, Special Publications, v. 245, p. 165 - 186.

Ritter, O., Weckmann, U., Hoffmann-Rothe, A., Abueladas, A., and Garfunkel, Z., DESERT Research Group, 2003, Geophysical images of the Dead Sea Transform in Jordan reveals an impermeable barrier for fluid flow Geophysical Research Letters, v. 30.

Rosendahl, B.R., 1987, Architecture of the continental rifts with special reference to East Africa: Annual Reviews of Earth and Planetary Sciences, v. 15, p. 445 - 503.

Schwartz, M.O., and Akanyang, P., 1994, Geological Map of Ngwako Pan: Geological Survey Botswana, scale 1:125000.

Sebagenzi, M.N., and Kaputo, K., 2002, Geophysical evidence of continental break up in the southeast of the Democratic Republic of Congo and Zambia (Central Africa) In: S.A.P.L. Cloetingh and Z. Ben-Avraham (Eds.), From continental extension to collision: Africa - Europe interaction, the Dead Sea and analogue natural laboratories: EGU (European Geosciences Union), Stephan Mueller Special Publication Series, v. 2, p. 193 - 206.

Sebagenzi, M.N., Vasseur, G., and Louis, P., 1993, First heat flow density determinations from southeastern Zaire (central Africa): Journal of African Earth Sciences, v. 16, p. 413 - 423.

Shaw, P., 1985, Late Quaternary Landforms and Environmental-Change in Northwest Botswana - the Evidence of Lake Ngami and the Mababe Depression: Transactions of the Institute of British Geographers, v. 10, p. 333 - 346.

Shaw, P., and Nash, D.J., 1998, Dual mechanisms for the formation of fluvial silcretes in the distal reaches of the Okavango Delta Fan, Botswana: Earth Surface Processes and Landforms, v. 23, p. 705 - 714.

Shemang, E.M., and Molwalefhe, L.N., 2009, DC Resistivity and Seismic Refraction Survey Across the SE Margin of Lake Ngami, NW Botswana: Acta Geophysica, v. 57, p. 728 - 742.

Stamps, D.S., Calais, E., Saria, E., Hartnady, C., Nocquet, J., Ebinger, C.J., and Fernandes, R.M., 2008, A kinematic model for the East African Rift: Geophysical Research Letters, v. 35, p. 1 - 6.

Suzuki, K., Toda, S., Kusunoki, K., Fujimitsu, Y., Mogi, T., and Jomori, A., 2000, Case studies of electrical and electromagnetic methods applied to mapping active faults beneath the thick quaternary: Engineering Geology, v. 56, p. 29 - 45.

Telford, W.M., Geldart, L.P., and Sherrif, R.E., 1990, Applied Geophysics: New York, Cambridge University Press, 770 p.

Teter, K., 2009, Paleoenvironmental reconstruction of Paleolake Mababe, northwestern Botswana from sediment chemistry and biological productivity data: Thesis (unpul), Oklahoma State University, p. 1 - 74.

Thomas, D.S.G., and Shaw, P.A., 1991, The Kalahari Environment: New York, Cambridge University Press, 284 p.

Thompson, D.T., 1982, EULDPH - A technique for making computer-assisted depth estimates for magnetic data: Geophysics, v. 47, p. 31 - 37.

Thurber, C., Roecker, S., Ellsworth, W., Chen, Y., Lutter, W., and Sessions, R., 1997, Two-dimensional seismic images of the San Andreas fault in the northern Gabilan Range, central California: evidence for fluids in the fault zone: Geophysical Research Letters, v. 24, p. 1591 - 1594.

Tournerie, B., and Chouteau, M., 2002, Analysis of magnetotelluric data along the Lithoprobe seismic line 21 in the Blake River Group, Abitibi, Canada: Earth Planets Space, v. 54, p. 575 - 589.

Townend, J., and Zoback, M.D., 2000, How faulting keeps the crust strong: Geology v. 28, p. 399 - 402.

Unsworth, M., and Bedrosian, P.A., 2004, Electrical resistivity structure at the SAFOD site from magnetotelluric exploration: Geophysical Research Letters, v. 31.

Unsworth, M.J., Bedrosian, P., Eisel, M., Egbert, G.D., and Siripunvaraporn, W., 2000, Along strike variations in the electrical structure of the San Andreas fault at Parkfield, California: Geophysical Research Letters, v. 27, p. 3021 - 3024.

Unsworth, M.J., Egbert, G.D., and Booker, J.R., 1999, High resolution electromagnetic imaging of the San Andreas fault in central California: Journal of Geophysical Research, v. 104, p. 1131 - 1150.

Unsworth, M.J., Malin, P.E., Egbert, G.D., and Booker, J.R., 1997, Internal structure of the San Andreas fault at Parkfield, California: Geology, v. 25, p. 359 - 362.

Vanneste, K., Verbeeck, K., and Petermans, T., 2008, Pseudo-3D imaging of low-slip-rate, active normal fault using shallow geophysical methods: The Geleen fault in the Belgian Maas River valley: Geophysics, v. 73, p. B1 - B9.

Whaler, K.A., and Hautot, S., 2006, The electrical resistivity structure of the crust beneath the northern Main Ethiopian Rift: Geological Society, London, Special Publications, v. 259, p. 293 - 305.

APPENDICES

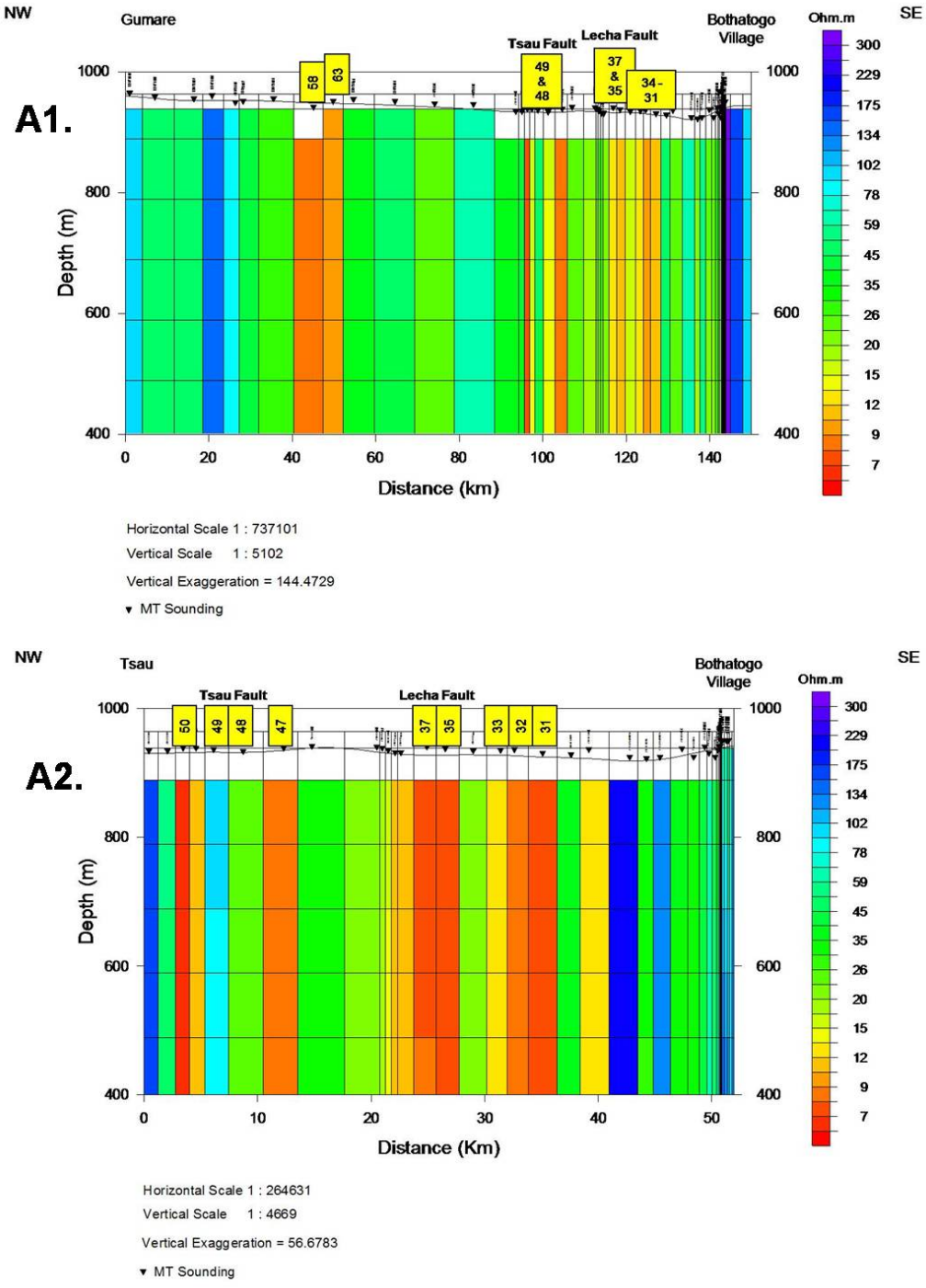

A1 and A2. MT 2D mesh inversion models displaying fault locations and vertical zones of conductivity along Profile 1. A2 is an enlarged area of MT model A1 to further investigate the conductive behavior of the Tsau and Lecha fault.

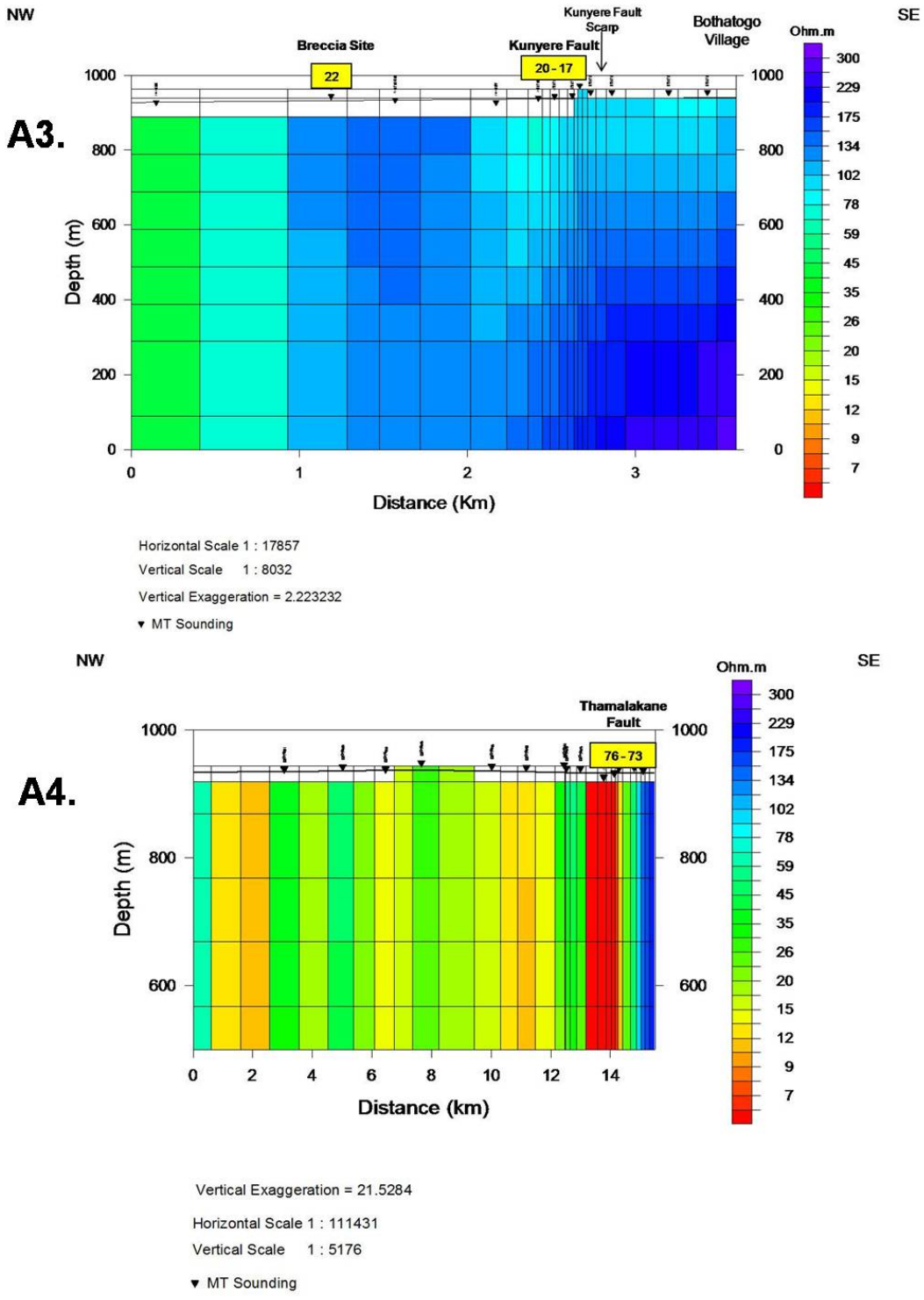

A3 and A4. MT 2D mesh inversion models displaying fault locations and vertical zones of conductivity. A3 is an enlarged area of MT model A1 to further investigate the conductive behavior of the Kunyere Fault. A4 is the MT 2D mesh inversion model for Profile 2.

VITA

Kelsey S. Mosley

Candidate for the Degree of

Master of Science

Thesis: GEOPHYSICAL CHARACTERIZATION OF FAULTS OF THE OKAVANGO RIFT ZONE, NORTHWEST BOTSWANA, AFRICA

Major Field: Geology

Biographical:

Education:

Completed the requirements for the Master of Science degree in Geology at Oklahoma State University, Stillwater, Oklahoma in May, 2010.

Completed the requirements for the Bachelor of Science degree in Geology at Oklahoma State University, Stillwater, Oklahoma in December, 2006.

Experience:

ConocoPhillips in Houston, TX

Professional Memberships:

American Association of Petroleum Geologists (AAPG)
Geological Society of America (GSA)
Society of Exploration Geophysicists (SEG)
National Association of Black Geologists and Geophysicists (NABGG)
American Geophysical Union (AGU)
Golden Key International Honour Society

Name: Kelsey S. Mosley Date of Degree: May, 2010

Institution: Oklahoma State University Location: Stillwater, Oklahoma

Title of Study: GEOPHYSICAL CHARACTERIZATION OF FAULTS OF THE OKAVANGO RIFT ZONE, NORTHWEST BOTSWANA, AFRICA

Pages in Study: 82 Candidate for the Degree of Master of Science

Major Field: Geology

Findings and Conclusions:

To examine the geophysical characteristics of the faults associated with the Okavango Rift Zone (ORZ) in northwest Botswana, electrical resistivity tomography (ERT), magnetotellurics (MT), total field magnetic, and gravity surveys were conducted along selected faults across the rift.

MT results show that the Tsau and Lecha faults have propagated into the sedimentary cover and are interpreted to be active conduits for fluid flow from the Okavango Delta despite their lack of surface expression. ERT and MT data show that tectonic activity along the Kunyere Fault has significantly waned and strain is being accommodated by the tectonically active Thamalakane Fault and Mababe Fault. Impermeable fault cores and an abundance of minor faults, fractures, and splays within the damage zones characterize the faults within the ORZ as both barriers and conduits to fluid flow. Ground and aeromagnetic data display some of the faults as magnetic highs while others are depicted as magnetic lows in the basement. The differences in magnetic character may be attributed to the 1.) commingling of fluids and basement rocks of contrasting redox potentials along fault planes or 2.) extreme variation of magnetic susceptibilities of the rocks juxtaposed on either side of the faults. Fluids may also play a role in increasing pore pressure through cracks associated with interconnecting faults and fractures, causing the ORZ to have a lack of severe earthquakes and allowing easier slip to occur between fault planes which may enhance lengthening the widening of the rift.

ADVISER'S APPROVAL: Dr. Estella Atekwana